

# 1            **EpiMix: an integrative tool for epigenomic**

## 2                            **subtyping using DNA methylation**

3

4    Yuanning Zheng<sup>1</sup>, John Jun<sup>1</sup>, Kevin Brennan<sup>1</sup> and Olivier Gevaert<sup>1</sup>

5

6    <sup>1</sup>Stanford Center for Biomedical Informatics Research (BMIR), Department of  
7    Medicine & Department of Biomedical Data Science, Stanford University, Stanford,  
8    CA 94305, USA

### 9

### 10    **Correspondence Information:**

11    Olivier Gevaert, Ph.D., Associate Professor

12    Stanford Center for Biomedical Informatics Research (BMIR)

13    Department of Medicine, Stanford University

14    1265 Welch Rd, Stanford, CA 94305-5479

15    Office: 650-721-2378

16    Email: [ogevaert@stanford.edu](mailto:ogevaert@stanford.edu)

17

18

19

20

21

22

## 23 **Abstract**

24

25 DNA methylation (DNAm) is a major epigenetic factor influencing gene expression  
26 with alterations leading to cancer, immunological, and cardiovascular diseases.  
27 Recent technological advances enable genome-wide quantification of DNAm in large  
28 human cohorts. So far, existing methods have not been evaluated to identify  
29 differential DNAm present in large and heterogeneous patient cohorts. We developed  
30 an end-to-end analytical framework named “EpiMix” for population-level analysis of  
31 DNAm and gene expression. Compared to existing methods, EpiMix showed higher  
32 sensitivity in detecting abnormal DNAm that was present in only small patient  
33 subsets. We extended the model-based analyses of EpiMix to cis-regulatory elements  
34 within protein-coding genes, distal enhancers, and genes encoding microRNAs and  
35 lncRNAs. Using cell-type specific data from two separate studies, we discovered novel  
36 epigenetic mechanisms underlying childhood food allergy and survival-associated,  
37 methylation-driven non-coding RNAs in non-small cell lung cancer.

38

39

40

41

42

43

44

45

46

## 47 **Main text**

48

49 DNA methylation (DNAm) is one of the major epigenetic marks in humans. It is  
50 defined as the addition of a methyl (CH<sub>3</sub>) group to DNA that occurs primarily at the  
51 cytosine of cytosine-guanine dinucleotide (CpG) sequence. DNAm regulates various  
52 biological processes by affecting gene expression, and aberrant DNAm plays a  
53 critical role in the development and progression of many human diseases<sup>1-3</sup>. Recent  
54 experimental methods based on microarrays or next-generation sequencing have  
55 enabled genome-wide quantification of DNAm at single-nucleotide resolution. Due to  
56 its quantitative and cost-effective nature, microarray-based technology has emerged  
57 as the method of choice for profiling DNAm in large human cohorts. For example,  
58 The Cancer Genome Atlas (TCGA) project has used the microarray technology to  
59 generate DNAm profiles in over 10,000 specimens representing 33 cancer types.  
60 The Gene Expression Omnibus database (GEO) and other public repositories also  
61 host a large number of DNAm datasets across cancers and other complex diseases.

62

63 Over the last decade, a number of computational approaches have been developed  
64 to identify genes that are abnormally methylated in human diseases. Some methods  
65 are tailored to the analysis of DNAm data from bisulfite sequencing<sup>4-7</sup>, while others  
66 are designed for array-based data or can be adapted to both data platforms<sup>8-12</sup>. Many  
67 existing methods identify differentially methylated loci by comparing all samples from  
68 an experimental group versus samples in a control group. This type of comparison  
69 works well when the experimental population is assumed to be homogenous. However,  
70 when the study population is large, abnormal DNAm may be present in only a subset

71 of the patients, and this intra-population variation has been observed in cancers and  
72 many other diseases<sup>13–15</sup>. In cases where abnormal DNAm occurred in only a small  
73 subset of the patients, existing methods are not capable of capturing the signals of  
74 differential methylation. Therefore, there is a critical need to use a statistical approach  
75 to model the distribution of DNAm in large patient cohorts, and to identify the patient  
76 subsets with differential DNAm profiles. This epigenetic subtyping can be essential  
77 to improve personalized diagnosis, treatment and drug discovery.

78

79 Furthermore, gene expression in mammalian cells is a result of a complex process  
80 coordinated by a broad range of genomic regulatory elements<sup>16,17</sup>. In many studies,  
81 CpG sites were mapped to genes based on linear genomic proximity. This mapping  
82 logic assumes that the transcriptional activity can be affected only when the genes are  
83 overlapped or close to the differentially methylated sites. However, emerging evidence  
84 has shown that distal enhancers, which may locate at a great linear genomic distance  
85 from their target genes, play a critical role in orchestrating spatiotemporal gene  
86 expression programs<sup>18</sup>. Abnormal DNAm at enhancers was frequently reported in  
87 cancers and many other diseases<sup>19,20</sup>. Therefore, the analysis of enhancer  
88 methylation can improve our understanding of how gene expression is regulated  
89 across physiological and pathological conditions.

90

91 Existing computational tools focus on the DNAm analysis of protein-coding genes.  
92 Besides protein-coding genes, non-coding RNAs, such as microRNAs (miRNAs) and  
93 long non-coding RNAs (lncRNAs), play an important role in regulating cell  
94 functions<sup>21,22</sup>. Recent studies have shown that DNAm is a major epigenetic

95 mechanism regulating non-coding RNA expression<sup>23,24</sup>. With existing methods, it is  
96 challenging to decipher how DNAm regulates non-coding RNA expression.

97

98 Here, we present EpiMix, a comprehensive analytical framework for population-level  
99 analysis of DNAm and gene expression. EpiMix utilizes a model-based  
100 computational approach to identify abnormal DNAm at diverse genomic elements,  
101 including cis-regulatory elements within or surrounding protein-coding genes, distal  
102 enhancers, and genes encoding miRNAs and lncRNAs. In two separate studies, we  
103 showed that EpiMix identified novel methylation-driven pathways in T cells from  
104 childhood food allergy and methylation-driven non-coding RNAs in non-small cell lung  
105 cancer patients. To improve usability, we disseminated EpiMix's algorithms in  
106 Bioconductor<sup>25</sup>, enabling end-to-end DNAm analysis. Furthermore, we developed a  
107 web tool for interactive exploration and visualization of EpiMix's results  
108 (<https://epimix.stanford.edu>). Overall, EpiMix can be used to discover novel epigenetic  
109 biomarkers for disease subtypes and therapeutic targets for personalized medicine.

110

## 111 **Results**

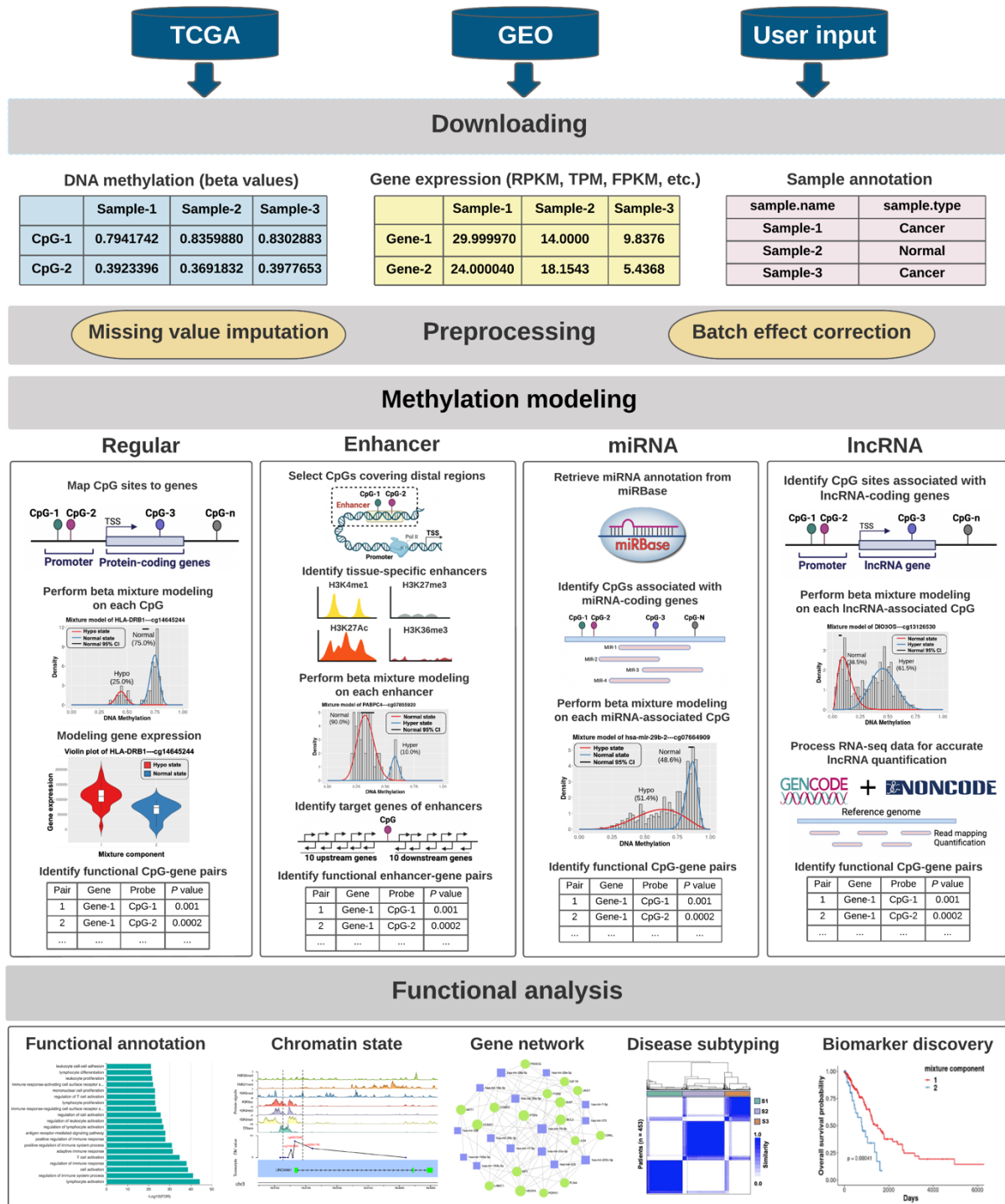
112

### 113 **Overview of EpiMix Workflow**

114

115 EpiMix is an end-to-end analytical framework for modeling DNAm at diverse genomic  
116 elements and for identifications of differential DNAm associated with gene  
117 expression. The EpiMix framework consisted of four functional modules: (1) data  
118 downloading, (2) preprocessing, (3) DNAm modeling and (4) functional analysis

119 **(Fig.1)**. To analyze DNAm at functionally diverse genomic elements, we  
120 implemented four alternative analytic modes: "Regular," "Enhancer", "miRNA" and  
121 "lncRNA." Both the Regular and Enhancer modes aimed to detect differential DNAm  
122 associated with the expression of protein-coding genes. The Regular mode analyzed  
123 DNAm sites within or immediately surrounding the genes, while the Enhancer mode  
124 specifically analyzed DNAm at distal enhancers. The miRNA and lncRNA modes  
125 were built for the detection of DNAm affecting the expression of miRNAs and  
126 lncRNAs. After the methylation-driven genes were identified, users could perform  
127 comprehensive exploratory analyses using the functional analysis module. The  
128 functional analysis module was built with both in-house developed methods and  
129 integrating existing computational tools to enable diverse functional analyses and  
130 visualization of the differential DNAm.

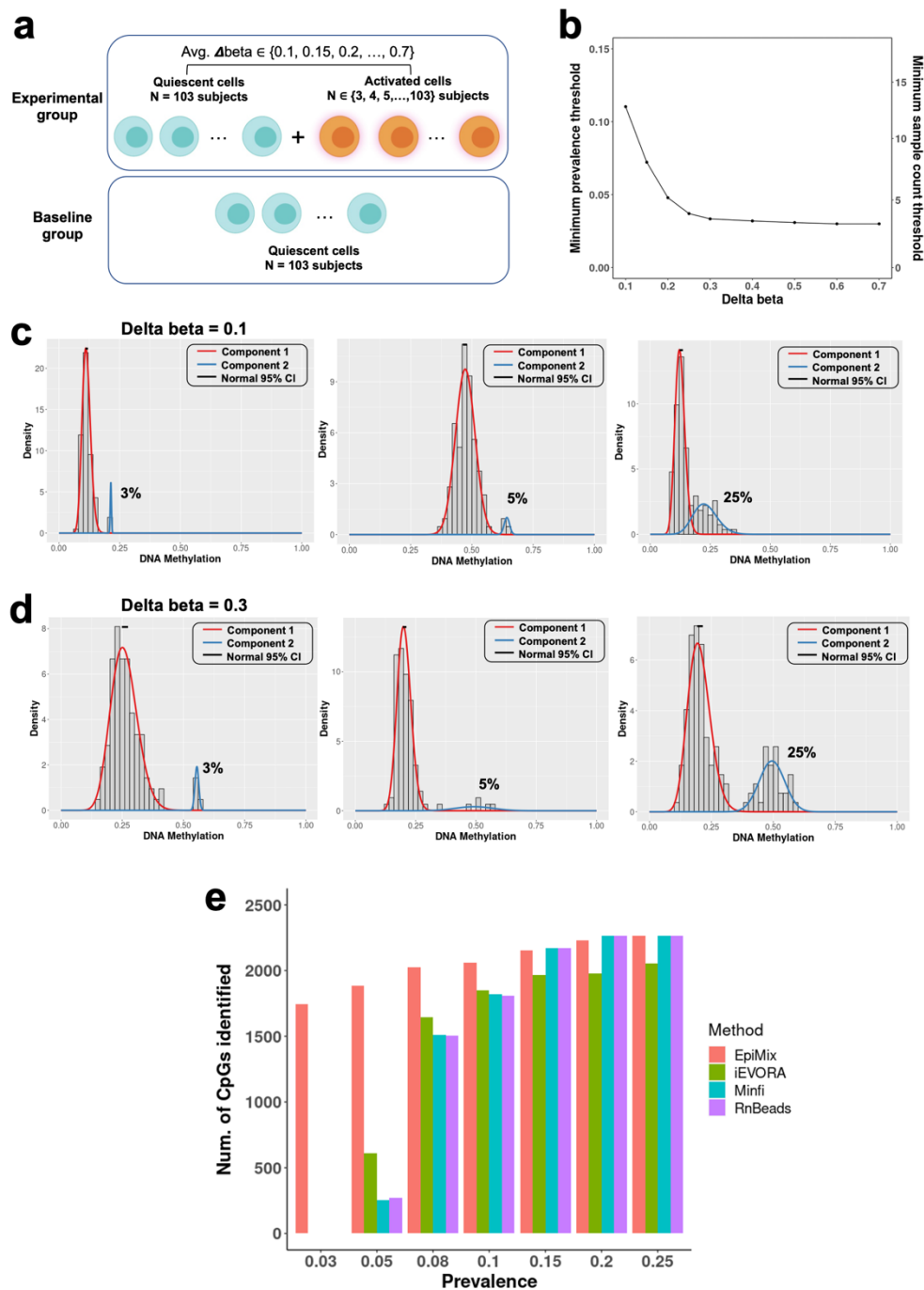


131 Fig.1 Overview of EpiMix workflow. EpiMix includes four modules: Downloading, Preprocessing, Methylation  
 132 modeling and Functional analysis. Data from public repositories (i.e., TCGA and GEO) can be automatically  
 133 downloaded and preprocessed by EpiMix. Alternatively, users can input their own custom datasets. The  
 134 preprocessing module includes functions for quality control, batch effect normalization, and missing value  
 135 imputation. To model DNAm, EpiMix enables four alternative analytic modes: Regular, Enhancer, miRNA and  
 136 lncRNA. Each mode uses a custom algorithm to analyze DNAm at a specific type of genomic element. One major  
 137 output from the methylation modeling is a matrix of functional CpG-gene pairs, illustrating the differentially  
 138 methylated CpGs whose DNAm states were associated with gene expression. After the differentially methylated  
 139 genes have been identified, users can perform diverse analytical tasks with EpiMix's functional analysis  
 140 module. This includes pathway enrichment analysis, genome-browser style visualization, gene regulatory network  
 141 analysis, epigenetic biomarker discovery and identification of methylation-associated disease subtypes.

## 143 **Identifications of abnormal DNAm present in small sample** 144 **subsets**

145

146 To assess the sensitivity of EpiMix in identifications of differential DNAm that was  
147 present in only specific patient subsets, we performed simulation experiments. We  
148 used a dataset that jointly profiled DNAm data and messenger RNA abundance in  
149 human naïve CD4+ T cells<sup>26</sup>. The dataset contains quiescent T cells and antigen-  
150 activated T cells from 103 human subjects. The DNAm data were obtained from  
151 Infinium MethylationEPIC array, and the messenger RNA expression data were  
152 obtained from RNA-Seq. We randomly sampled a subset of CpGs ( $n = 300$ ) from the  
153 quiescent group as baselines, such that the average beta values of the selected CpGs  
154 ranged from 0.1 to 0.9. Then, for each CpG, we randomly selected a subset of samples  
155 from the activation group and combined them with the baseline group (**Fig.2a** and  
156 **Methods**), such that the final proportions of samples from the activation group in the  
157 combined dataset ranged from 3% to 50%, and the mean differences in beta values  
158 between the activated and the baseline samples ranged from 0.1 to 0.7. We then  
159 compared the DNAm of the synthetic populations to the baseline population (**Fig.2a**).



160

161 Fig.2 a, Design of the simulation study. The dataset contained experimentally purified naïve CD4+ T cells from 103  
 162 human subjects. Cells from each subject were divided into half and either activated with the T-cell antigen or left  
 163 resting in the media. The baseline group contained quiescent samples from all 103 subjects. The experimental  
 164 group contained quiescent samples from all subjects and the antigen-activated samples from  $N$  subjects, where  $N$   
 165 ranged from 3 to 103. We compared the DNAm of the experimental group to the baseline group and tested  
 166 whether EpiMix can detect the signals of differential methylation. **b**, Correlation between the delta beta values and  
 167 the minimum detection threshold for the prevalence (left axis) and actual count (right axis) of the activated samples  
 168 in the experimental group. The simulation was repeated 300 times using a different CpG site at each time, and the  
 169 mean detection threshold was shown. **c**, Density plots showing the mixture models when delta beta was 0.1 and  
 170 the differential methylation was present in 3%, 5% and 25% of the experimental group. **d**, Density plots showing  
 171 the mixture models when delta beta was 0.3 and the differential methylation was present in 3%, 5%, and 25% of  
 172 the experimental group. **e**) Number of differentially methylated CpGs detected by different methods when the  
 173 differential methylation was present in from 3% to 25% of the population. For all methods, the same set of CpGs  
 174 were used, and the total number of CpGs at each prevalence was 2,700.

175

176 We found that the sensitivity of EpiMix was determined by the magnitude of differences  
177 in DNAm between the quiescent and the activated subjects. When the delta beta was  
178 0.1, EpiMix detected differential DNAm that was present in 3% to 25% of the synthetic  
179 population, with a mean minimum detection threshold of 11.0% (absolute sample  
180 count = 13) (**Fig.2b, c**). When the delta beta was 0.2 or higher, the minimum detection  
181 threshold ranged from 3% to 10%, with a mean threshold of 3.4% (absolute sample  
182 count = 4) (**Fig.2b, d**). These results indicated that EpiMix was able to detect abnormal  
183 DNAm that was present in only small subsets of a tested population, and the  
184 sensitivity was positively correlated with the magnitude of differences in DNAm.

185

186 Next, we compared the performance of EpiMix with other existing methods in  
187 identifications of differential DNAm, including Minfi<sup>10</sup>, iEVORA<sup>27</sup> and RnBeads<sup>12,28</sup>.  
188 When the differential DNAm was present in 3% of the population, EpiMix detected  
189 the differential methylation signals at 1,747 CpG sites, whereas the other methods did  
190 not capture any differential DNAm (**Fig.2e**). When the differential DNAm was  
191 present in 5% of the population, EpiMix identified 3.1 times more differentially  
192 methylated CpGs than iEVORA, and 3.6 times more CpGs than Minfi and RnBeads.  
193 Minfi and RnBeads only detected CpGs with high magnitude differences in DNAm,  
194 with an average delta beta of 0.6. In contrast, EpiMix detected CpGs with delta beta  
195 ranging from 0.1 to 0.7, with an average threshold of 0.3. When the prevalence of  
196 differential DNAm was 15% or higher, EpiMix detected similar numbers of CpGs to  
197 the other three methods. These results indicated that EpiMix had higher sensitivity to  
198 detect differential DNAm that was present in only small sample subsets.

199

## 200 **Modeling of DNA methylation at *cis*-regulatory elements within** 201 **protein-coding genes**

202

203 To test the Regular mode of EpiMix, we used the complete, real dataset from antigen-  
204 activated T cells and quiescent T cells (n = 103 subjects per group)<sup>26</sup>. In the activated  
205 T cells, 1,090 CpGs were differentially methylated compared to the quiescent cells.  
206 Integrative analysis with RNA-seq data showed that the differentially methylated CpGs  
207 were functionally associated with the expression of 748 protein-coding genes  
208 (**Supplementary Table 1**). Of the differentially methylated CpGs, 746 (68.4%) CpGs  
209 associated with 504 genes were hypomethylated and 327 (30.0%) CpGs associated  
210 with 238 genes were hypermethylated (**Fig.3a**). This result indicated that antigens  
211 induced a widespread loss of DNAm. Gene ontology (GO) analysis showed that the  
212 hypomethylated genes were associated with lymphocyte proliferation (e.g., *CCND2*,  
213 *CCND3*, *CDK6*, *CDK14*), T cell activation (e.g., *BCL2*, *CCL5*, *HLA-DPA1*, *HLA-DRB1*),  
214 glycoprotein biosynthesis (e.g., *AGO2*, *ALG9*, *B3GNT5*, *B4GALT5*) and cytokine  
215 receptor activity (*IL1R1*, *IL1R2*, *IL21R*, *IL23R*) (**Supplementary Table 2**). This result  
216 confirmed that EpiMix identified differential DNAm associated with T cell activation.

217

218 Many of the CpGs were differentially methylated in only a subset of the patients. For  
219 instance, the *Human Leukocyte Antigen DRB1 (HLA-DRB1)* gene was  
220 hypomethylated in the antigen-activated T cells from 25% of the subjects, whereas the  
221 majority (75%) of the subjects had a normal methylation state similar to the quiescent  
222 T cells (**Fig.3b**). As expected, gene expression levels of *HLA-DRB1* were significantly  
223 increased in the hypomethylated compared to the normally methylated subjects  
224 (**Fig.3c**). Overall, the prevalence of hypomethylation ranged from 5.9% - 100%, with

225 a mean prevalence of 69.6% (**Fig.3d**). The prevalence of hypermethylation ranged  
226 from 5.8% - 100%, with a mean prevalence of 47.3% (**Fig.3e**). These results indicated  
227 that the antigen-induced response in T cells varied between different individuals.

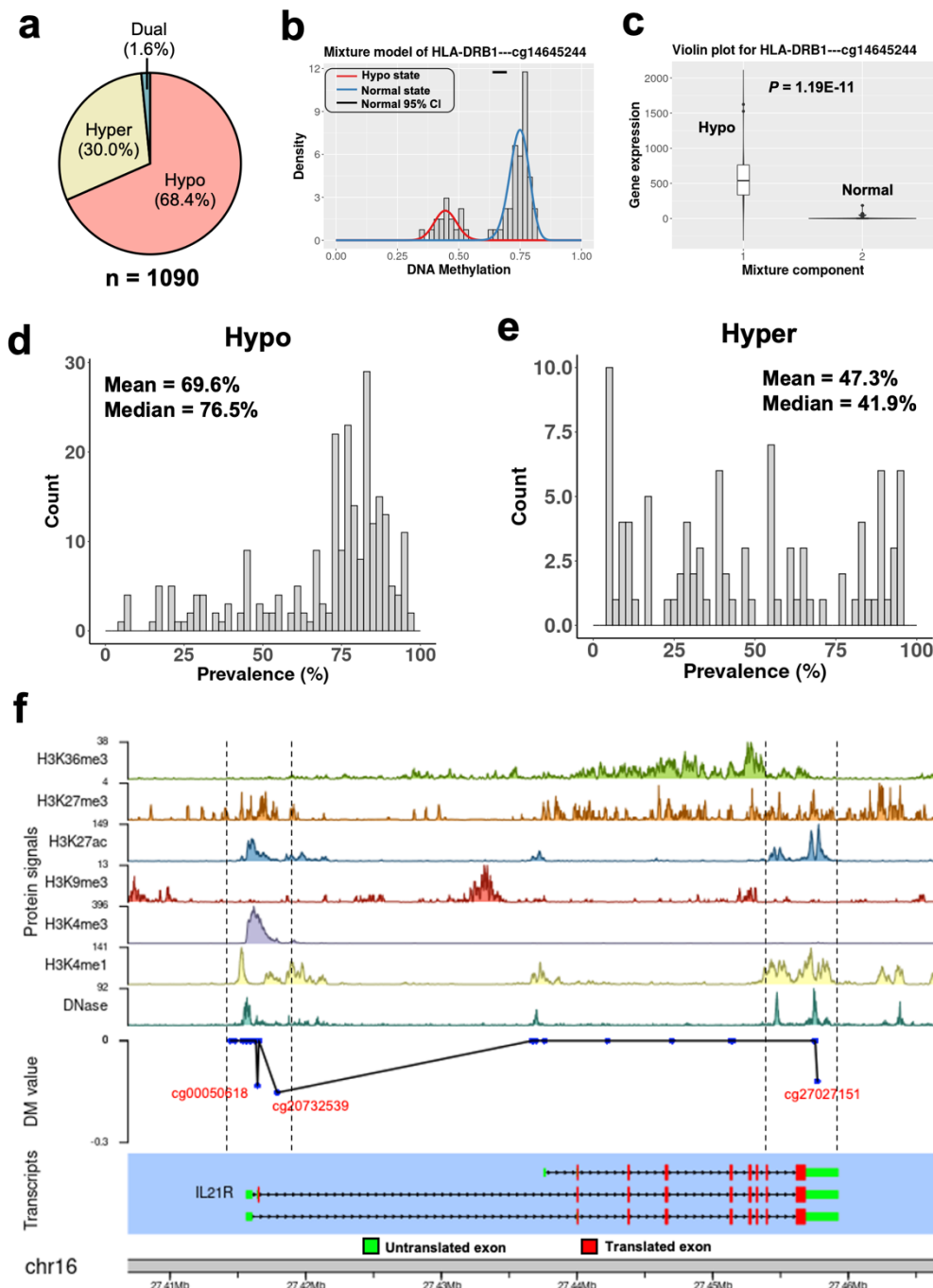
228

229 We next investigated the genomic distribution of the differentially methylated CpGs.  
230 Thirty-nine percent (39.5%) of the CpGs were located at the promoters, and 56.4%  
231 were located at introns (**Supplementary Fig.1a**). Using publicly available chromatin  
232 immunoprecipitation-sequencing (ChIP-seq) data of human naïve CD4+ T cells, we  
233 found that the abnormal DNAm was significantly enriched at active promoters  
234 marked by H3K4me3 and H3K27ac, active enhancers marked by H3K4me1, and to a  
235 lesser extent, actively transcribed gene bodies marked by H3K36me3  
236 (**Supplementary Fig.1b**). These results demonstrated that EpiMix was able to identify  
237 aberrant DNAm at lineage-defining *cis*-regulatory elements.

238

239 To allow users to investigate the genomic locations and chromatin states associated  
240 with the differentially methylated sites, EpiMix enables genome browser-style  
241 visualization. We illustrated this functionality with hypomethylation in two regions of  
242 the interleukin-receptor gene *IL21R* (**Fig.3f**). The first region was located at the  
243 promoter, which overlapped with DNase I hypersensitivity sites and activating histone  
244 modifications (i.e., H3K4me1, H3K4me3 and H3K27ac). The second region was  
245 located at the three-prime untranslated region, enriched with histone modifications  
246 marking for active enhancers (i.e., H3K4me1 and H3K27ac). In concordance with this  
247 DNA hypomethylation, *IL21R* expression levels were significantly increased  
248 (**Supplementary Table 1**, Wilcoxon rank-sum test,  $P < 3.19E-08$ ).

249



250 **Fig.3 Identifications of differential DNAm resulting from antigen-induced T cell activation.** **a**, Proportions  
 251 of the hypo-, hyper- and dual methylated CpGs in antigen-activated T cells. The dual methylated CpGs refer to the  
 252 CpGs that were hypomethylated in some individuals, while hypermethylated in some other individuals. **b**, Mixture  
 253 model of a CpG associated with the *HLA-DRB1* gene, and **c**, *HLA-DRB1* gene expression levels in different  
 254 mixtures. Red indicates hypomethylation ( $n = 26$ ), while blue indicates normal methylation ( $n = 77$ ). Gene  
 255 expression levels were compared with Wilcoxon rank-sum test. **d-e**, Density plots showing the prevalence  
 256 distribution of the d) hypo- and e) hyper-methylated CpGs **f**, Genome-browser style visualization of the chromatin  
 257 state, DM values, and transcript structure of the *IL21R* gene. The hypomethylated CpGs were labeled in red. The  
 258 differential methylation (DM) value represents the mean difference in beta values between the hypomethylated  
 259 subjects versus the normally methylated subjects. DM = 0: normal methylation; DM < 0: hypomethylation.

260

## 261 Identification of functional DNA methylation at distal enhancers in food allergy

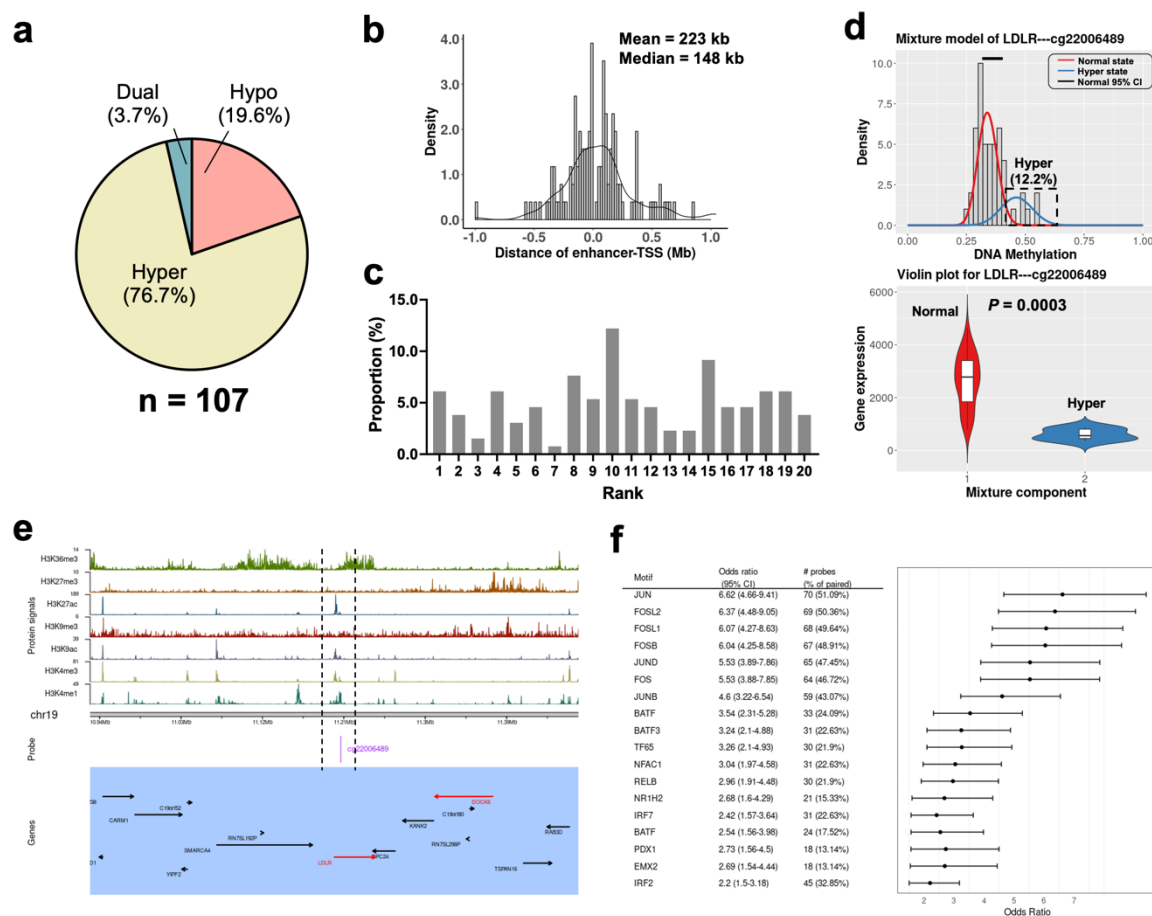
262

263 To demonstrate the Enhancer mode of EpiMix, we used the same CD4+ T cell  
264 dataset<sup>26</sup>. In this dataset, 82 human subjects were diagnosed with food allergy and 21  
265 subjects were non-allergic controls. The differential response of T cells to antigen-  
266 induced activation between different individuals may be associated with the allergic  
267 status. We then characterized allergy-associated changes in DNAm by comparing  
268 antigen-activated T cells from the allergic patients to those from the non-allergic  
269 controls. Using a permutation approach (**Supplementary Fig.2** and **Methods**), we  
270 identified 107 differentially methylated enhancers that were functionally linked to the  
271 expression of 119 genes. The number of target genes of each enhancer ranged from  
272 1 to 3, resulting in 131 significant enhancer-gene pairs (**Supplementary Table 3**).  
273 This result is consistent with the previous studies showing that enhancers typically  
274 loop to and are associated with the activation of 1 to 3 promoters<sup>29,30</sup>. Of the functional  
275 enhancers, 21/107 (19.6%) enhancers associated with 24 genes were  
276 hypomethylated, 82/107 (76.7%) enhancers associated with 92 genes were  
277 hypermethylated (**Fig.4a**). This result indicated that there was a global gain of DNAm  
278 at enhancers in food allergy.

279

280 The genomic distance between enhancers and their target genes ranged from 4.5 kb  
281 to 1.7 Mb, with a median distance of 148 kb (**Fig.4b**). In a previous study, Jin et al.  
282 used high-throughput chromosome conformation capture (Hi-C) assay to investigate  
283 promoter-enhancer interactions and demonstrated that approximately 25% of the  
284 enhancer-promoter pairs are within a 50 kb range and approximately 57% spans 100  
285 kb or greater genomic distance, with a median distance of 124 kb<sup>31</sup>. Another study by

286 Rao et al. showed that the distance between enhancers and promoters spans from 40  
 287 kb to 3 MB, with a median distance of 185 kb<sup>32</sup>. Our data agree with these  
 288 experimentally generated results. To further characterize the enhancer-gene linkage,  
 289 we investigated how often did the functional enhancers associate with the nearest  
 290 gene promoter. We ranked the 20 adjacent genes of each enhancer by their genomic  
 291 distance to the enhancer. **Fig.4c** showed that only 6.1% of the times did the enhancer  
 292 associate with the nearest promoter, whereas the majority of the enhancers skipped  
 293 one or more intervening genes to associate with promoters farther away. In line with



294 **Fig. 4** Identifications of differentially methylated enhancers associated with food allergy. **a**, Proportions of  
 295 the hypo-, hyper- and dual methylated enhancers in children with food allergy. **b**, Distribution of the linear genomic  
 296 distance between enhancers and their gene targets. **c**, For each functional enhancer, the 20 adjacent genes were  
 297 ranked by genomic distance. Bars show the proportions of the functionally linked genes in each rank. **d**, Mixture  
 298 model of the *LDLR* gene (top panel) and *LDLR* gene expression levels in different mixtures (bottom panel). Red  
 299 indicates normal methylation ( $n = 72$ ), while blue indicates hypermethylation ( $n = 10$ ). Gene expression levels were  
 300 compared by Wilcoxon rank-sum test. **e**, Integrative visualization of the chromatin states and the adjacent genes  
 301 of the hypermethylated enhancer shown in panel d. The genes in the functional CpG-gene pairs are shown in red,  
 302 while the others are shown in black. **f**, Enriched TF motifs and odds ratios for the differentially methylated enhancers.  
 303 To find significantly enriched motifs, we used all the distal CpGs as the background and the functional enhancers  
 304 as the targets.

305 this result, a previous study using the chromosome 5C assay showed that only ~7%  
306 of the time did the distal elements loop to the promoter of the nearest gene, whereas  
307 the majority of enhancers bypass the nearest promoter and loop to promoters farther  
308 away<sup>33</sup>. These results confirmed that EpiMix identified true distal *cis*-regulatory events.

309

310 The genes linked to the differentially methylated enhancers were related to the lipid  
311 metabolism (*LDLR*, *CAT*, *LPIN2*, *SREBF1*, *PIK3C2B*) and T cell activation (*CASP3*,  
312 *MALT*, *PRKCZ*, *SMAD3*). **Fig.4d** showed that the enhancer linked to the *LDLR* gene  
313 was hypermethylated in 12.2% of the allergic patients, and the gene expression of  
314 *LDLR* was significantly decreased in the hypermethylated patients. Integrative  
315 visualization (**Fig.4e**) showed that the hypermethylated enhancer overlapped with the  
316 Dnase I hypersensitivity site and was enriched with histone modifications marking for  
317 active enhancers, including H3K4me1 and H3K27ac, and to a lesser extent, H3K4me3  
318 and H3K9ac. The *LDLR* gene encodes a low-density lipoprotein receptor that  
319 transports cholesterol from the blood into the cell, which plays a critical role in  
320 regulating T cell lipid metabolism<sup>34</sup>. Our results suggested that T cells from a small  
321 subset of the allergic patients may have an abnormal lipid metabolic profile due to  
322 enhancer hypermethylation.

323

324 Enhancers are enriched for sequences bound by site-specific transcription factors  
325 (TFs). Hypermethylation of enhancers suppresses gene transcription by decreasing  
326 the binding affinity of TFs<sup>35,36</sup>. We then carried out motif enrichment analysis of the  
327 differentially methylated enhancers. We identified significant enrichment of binding  
328 sites for Jun-related factors (*JUN*, *JUND*), Fos-related factors (*FOS*, *FOSL1*, *FOSL2*,  
329 *FOSB*), BATF-related factors (*BATF*, *BATF3*), and Interferon-regulatory factors (*IRF2*,

330 IRF5, IRF7) (**Fig.4f** and **Supplementary Table 4**). These results agree with the  
331 evidence showing that Jun-related factors, BATF-related factors and Interferon-  
332 regulatory factors play a critical role in regulating the immune gene activation in T cells,  
333 and dysregulation of their activity causes aberrant immune response<sup>37,38</sup>. Our results  
334 demonstrated that the abnormal DNAm at enhancers affected the target gene  
335 response of these TFs and increased the subsequent risk for developing food allergy.

336

### 337 **Identification of methylation-driven miRNAs in human lung cancer**

338

339 Similar to protein-coding genes, miRNA-coding genes are transcriptionally regulated  
340 by DNAm<sup>39,40</sup>. To demonstrate the miRNA mode of EpiMix, we used a lung  
341 adenocarcinoma dataset containing DNAm and miRNA expression profiles of 457  
342 tumors and 32 adjacent normal tissues<sup>41</sup>. The DNAm data were acquired from the  
343 HM450 array, and the gene expression data were obtained from high-throughput  
344 microRNA sequencing (miRNA-Seq).

345

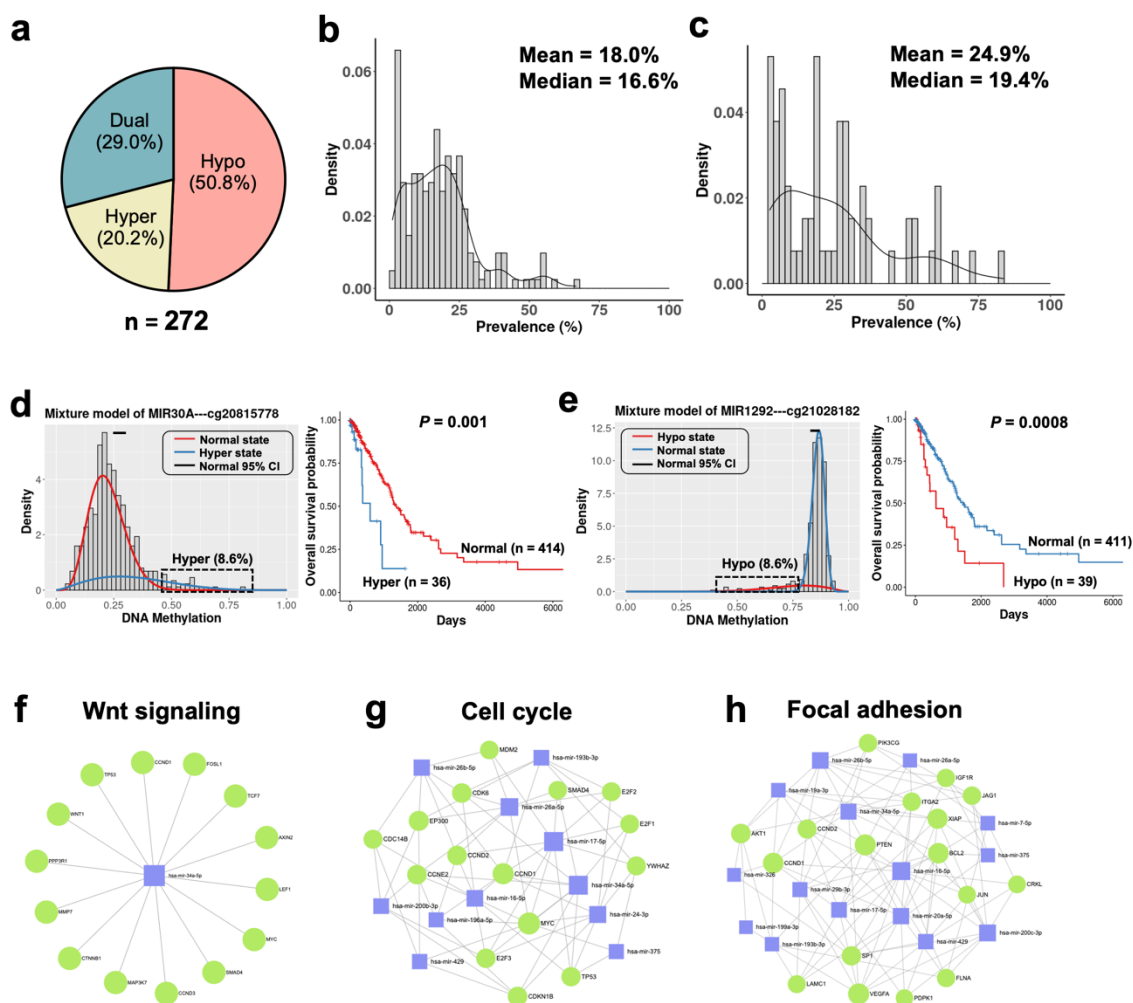
346 Both tumors and normal tissues from the lung are composed of multiple cell types,  
347 majorly including epithelial cells, fibroblasts, hematopoietic cells and endothelial cells.  
348 Studies have shown that DNAm profiles are cell-type specific<sup>42,43</sup>. When using data  
349 collected at the tissue (“bulk”) level for DNAm analysis, the differential DNAm may  
350 result from variations in cell-type proportions between different individuals. To resolve  
351 the confounding effects from intra-tumoral heterogeneity, we used previously  
352 validated computational methods to decompose tissue compositions and to infer cell-  
353 type-specific methylomes and transcriptomes (**Supplementary Fig. 3** and  
354 **Methods**)<sup>44,45</sup>. We then applied EpiMix to the deconvoluted data of each individual cell

355 type. In epithelial cells, we identified 272 differentially methylated CpGs functionally  
356 associated with the expression of 92 miRNA genes (**Fig.5a** and **Supplementary**  
357 **Table 5**). In fibroblasts, we found 12 hypomethylated CpGs functionally associated  
358 with the expression of 3 miRNA genes (**Supplementary Fig. 4a-b**). Although we  
359 discovered 9 differentially methylated CpGs in hematopoietic cells and 6 CpGs in  
360 endothelial cells, none of the differential DNAm were functionally correlated with  
361 gene expression. We further compared the differentially methylated gene lists  
362 identified using data from bulk tissues versus the ones using individual cell types. Over  
363 80% of the differentially methylated genes identified in epithelial cells could also be  
364 identified using data from bulk tissues (**Supplementary Fig. 4a-b**). These results  
365 demonstrated that, although tumors are composed of multiple cell types, the majority  
366 of differential methylation events occurred in epithelial cells.

367

368 We next focused our analysis on the deconvoluted data of epithelial cells. Of the 272  
369 differentially methylated CpGs, 138 (50.8%) CpGs associated with 66 genes were  
370 hypomethylated and 55 (20.2%) CpGs associated with 37 genes were  
371 hypermethylated. Sixty-five percent (63.6%) of the functional CpGs were located at  
372 the promoters, and this proportion was significantly higher than randomly selected  
373 CpGs (**Supplementary Fig.1c**, Fisher's exact test,  $P = 0.003$ ). Using publicly available  
374 ChIP-seq data of lung, we further determined that the differentially methylated regions  
375 were enriched with histone modifications (i.e., H3K27ac, H3K4me1 and H3K4me3)  
376 marking for actively transcribed promoters and enhancers (**Supplementary Fig.1d**).  
377 The prevalence of hypomethylation ranged from 1.1% to 66.7%, with a mean  
378 prevalence of 18.0% (**Fig. 5b**). Similarly, the prevalence of hypermethylation ranged  
379 from 2.6% to 83.7%, with a mean prevalence of 24.9% (**Fig. 5c**). These results

380 indicated that the majority of differential DNAm associated with miRNA genes  
 381 occurred in less than 25% of the patient population.



382 **Fig. 5** Identifications of differentially methylated miRNA-coding genes in human lung cancers. **a**, Proportions  
 383 of the hypo-, hyper- and dual methylated CpGs of miRNAs in lung cancer. **b-c**, Density plots showing the  
 384 prevalence distribution of the differentially methylated miRNAs in lung cancers ( $n = 457$ ), **(b)** prevalence of  
 385 hypomethylation and **(c)** prevalence of hypermethylation. **d**, Mixture model of the *MIR30A* gene (left panel) and  
 386 Kaplan-Meier survival curves of patients in different mixtures (right panel). Red indicates normal methylation and  
 387 blue indicates hypermethylation. Gene expression levels were compared by Wilcoxon rank-sum test. **e**, Mixture  
 388 model of the *MIR1292* gene (left panel) and Kaplan-Meier survival curves of patients in different mixtures (right  
 389 panel). Red indicates hypomethylation and blue indicates normal methylation. **f-g-h**, Network visualization of **(f)**  
 390 the gene targets of miR-34a, **(g)** differentially methylated miRNAs related to the cell cycle pathway, and **(h)** focal  
 391 adhesion pathway. Blue squares: miRNAs, green circles: protein-coding genes targeted by miRNAs.

392

393 MicroRNAs play an important role in regulating cell proliferation, invasion and cancer  
 394 metastasis<sup>46,47</sup>. We next investigated whether the DNAm of miRNAs were associated  
 395 with patient survival. Of the 92 methylation-driven miRNAs, we identified 22 miRNAs  
 396 whose methylation states were significantly correlated with patient survival

397 **(Supplementary table 6**, log-rank test,  $P < 0.05$ ). Half (11/22, 50%) of the survival-  
398 associated miRNAs were hypomethylated and the others (11/22, 50%) were  
399 hypermethylated. Some of the miRNAs, such as *MIR29C*<sup>48</sup>, *MIR30A*<sup>49</sup>, *MIR34A*<sup>50</sup> and  
400 *MIR148A*<sup>51</sup>, were known to be associated with lung cancer survival. For instance,  
401 *MIR30A*, a tumor suppressor miRNA<sup>49</sup>, was hypermethylated in 8.6% of the patients,  
402 and the hypermethylated patients showed a significantly worse survival than the  
403 normally methylated patients (**Fig.5d**, Hazard Ratio = 1.50,  $P = 0.001$ ). In addition,  
404 EpiMix identified many new survival-associated miRNAs. For instance, *MIR1292* was  
405 hypomethylated in 8.6% of the patients, and the hypomethylated patients showed  
406 significantly worse survival (**Fig.5e**, Hazard Ratio = 1.39,  $P = 0.0008$ ). These results  
407 demonstrated that EpiMix was able to identify survival-associated miRNAs that were  
408 differentially methylated in only small subsets of the patients, and this feature can be  
409 used to discover novel epigenetic biomarkers for prognosis.

410

411 To gain systematic insight into the biological functions of the methylation-driven  
412 miRNAs, we queried miRTarBase<sup>52</sup> to obtain experimental validated target genes of  
413 the miRNAs. We then performed pathway analyses of the target gene list. The  
414 differentially methylated miRNAs were related to Wnt signaling pathway, cell cycle,  
415 p53 signaling, focal adhesion and apoptosis (**Fig.5f-h** and **Supplementary Table 7**).  
416 These results provided mechanistic insights into how abnormal DNAm of miRNAs  
417 was involved in the development and progression of lung cancer. The data also  
418 suggested that targeting miRNA expression can be a therapeutic strategy to inhibit  
419 tumor progression and to improve patient survival.

420

421 **Identification of methylation-driven lncRNAs in human lung cancer**

422

423 To demonstrate the lncRNA mode of EpiMix, we used the same lung adenocarcinoma  
424 dataset<sup>41</sup>, and we aimed to identify differentially methylated lncRNA genes in tumors  
425 compared to normal tissues. Compared to protein-coding genes, lncRNAs are shorter,  
426 lower-expressed, less evolutionarily conserved, and expressed in a more tissue-  
427 specific manner<sup>53</sup>. To precisely quantify lncRNA expression from RNA-Seq, we used  
428 our previously developed pipeline<sup>54</sup>. With this pipeline, we combined the transcriptome  
429 annotations from GENCODE and NONCODE<sup>55</sup>. Raw sequencing reads were aligned  
430 to the combined transcriptome reference and quantified using the Kallisto-Sleuth  
431 algorithm<sup>56,57</sup>. Using this pipeline, we were able to detect the expression of 2,475  
432 lncRNAs in both tumors and normal tissues. This number was three times higher  
433 compared to the lncRNAs detected by the traditional STAR-HTSeq pipeline. We then  
434 computationally deconvoluted bulk DNAm data and lncRNA expression data to cell-  
435 type-specific data (**Supplementary Fig. 3**). Since over 95% of the functional  
436 differential DNAm was found in epithelial cells (**Supplementary Fig. 4c-d**), we next  
437 focused our analysis on epithelial cells.

438

439 EpiMix identified 397 CpGs functionally associated with the expression of 132  
440 lncRNAs in epithelial cells (**Fig.6a** and **Supplementary Table 8**). Of these CpGs, 146  
441 (36.8%) CpGs associated with 69 genes were hypomethylated and 187 (47.1%) CpGs  
442 associated with 73 genes were hypermethylated. Seventy-two percent (72.0%) of the  
443 functional CpGs were located at the promoters, and this proportion was significantly  
444 higher than randomly selected CpGs (**Supplementary Fig.1e**, Fisher's exact test,  $P$   
445  $< 0.0001$ ). The differentially methylated regions were enriched with histone

446 modifications marking for actively transcribed promoters and enhancers, including  
447 H3K27ac, H3K4me1 and H3K4me3 (**Supplementary Fig.1f**).

448  
449 The majority of differential methylation was identified in less 50% of the patients. The  
450 prevalence for hypomethylation ranged from 1.8% to 53.0%, with a mean value of 19.8%  
451 (**Fig.6b**). Similarly, the prevalence for hypermethylation ranged from 0.6% to 68.2%,  
452 with a mean value of 18.9% (**Fig.6c**). For instance, one of the hypermethylated  
453 lncRNAs was *LINC00881*. *LINC00881* was hypermethylated at CG11931463 in 15.7%  
454 of the patients and CG00673344 in 7.9% of the patients (**Fig.6d**). Both CpGs were  
455 located within the promoter (**Fig.6e**). Integrative analysis with clinical data showed that  
456 *LINC00881* hypermethylation was associated with significantly worse patient survival  
457 (**Figs.6f**, log-rank test,  $P < 0.001$ ). These data demonstrated that many lncRNAs were  
458 differentially methylated in only a subset of the lung cancer patients. In addition, EpiMix  
459 was able to identify survival-associated lncRNAs that were differentially methylated in  
460 small patient subsets.

461  
462 One of the major outputs from EpiMix is a differential methylation or “DM” value matrix,  
463 which reflects the homogeneous subpopulations of samples with a particular  
464 methylation state (**Fig.6g**). An application of the DM value matrix is to identify DNAm-  
465 associated subtypes, where patients are clustered into robust and homogenous  
466 groups based on their differential DNAm profiles. Using unsupervised consensus  
467 clustering, we discovered five DNAm subtypes (S1–S5) (**Fig.6h**). S5 contained a  
468 significantly higher proportion of females (89/133 = 66.9%) compared to S1 (54/120 =  
469 45.0%), S2 (36/74 = 48.6%) and S4 (16/50 = 32.0%) (**Fig.6i**, Fisher’s exact test,  $P <$   
470 0.01). In addition, patients from S5 had significantly better survival than patients of S2

471 **(Fig.6j, log-rank test,  $P = 0.007$ )**. We benchmarked the clustering results from using  
472 the DM value matrix versus using the raw DNAm data (beta values) of the  
473 differentially methylated CpGs. The patient subsets identified using raw DNAm data  
474 had low cluster consensus (**Supplementary Fig.5**), and no significant association was  
475 found between patient subsets and survival outcome. These results demonstrated that  
476 the DNAm subtypes discovered by EpiMix had prognostic values.

477

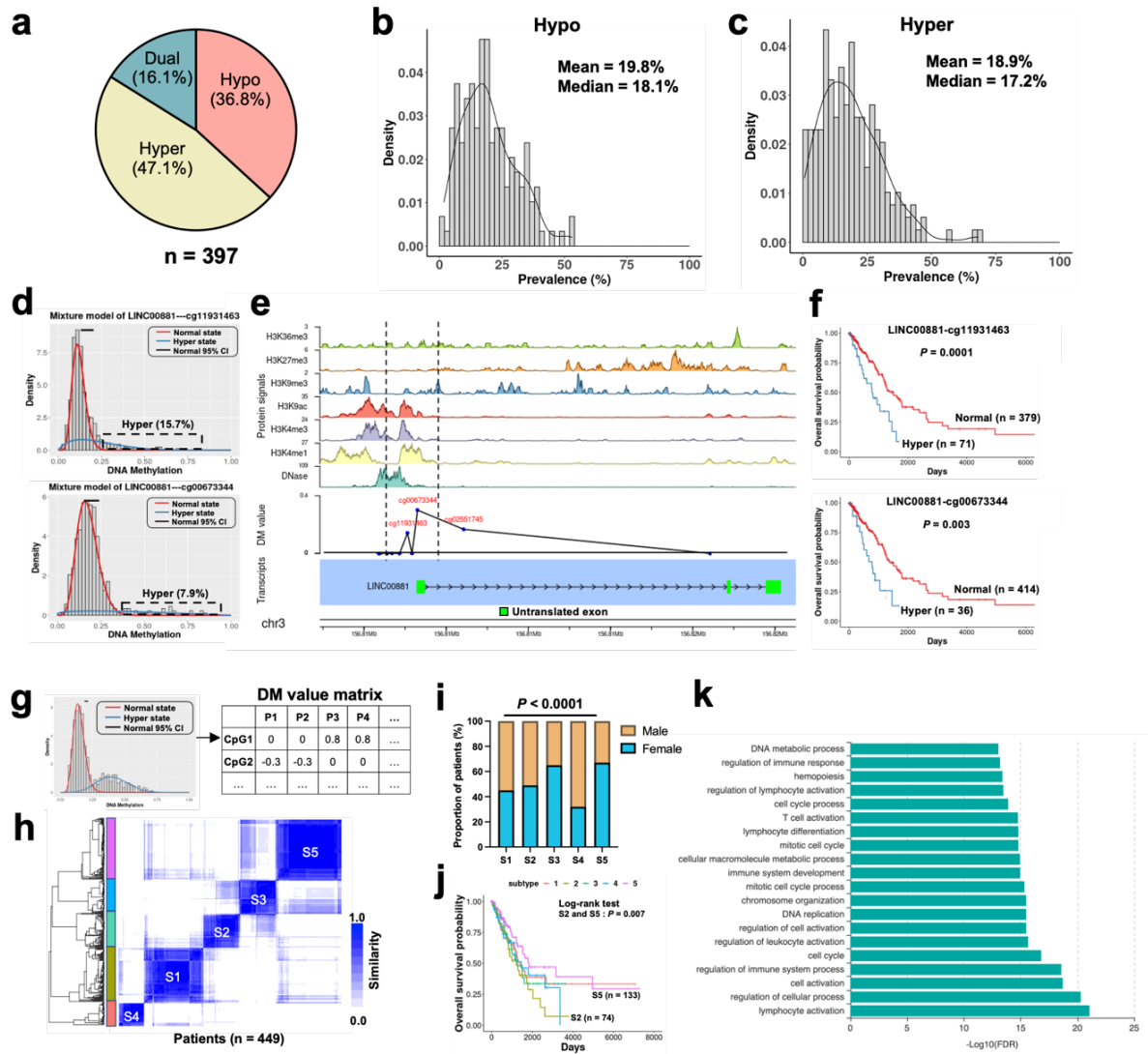
478 To investigate the biological functions of the differentially methylated lncRNAs, we  
479 utilized ncFANs, a functional annotation tool for lncRNAs<sup>58</sup>. We identified 4,552  
480 protein-coding genes functionally associated with 76 lncRNAs. GO analysis showed  
481 that the protein-coding genes were primarily associated with DNA replication, cell  
482 cycle and regulation of cell activation (**Fig.6k and Supplementary Table 9**). These  
483 results indicated how differential methylation of lncRNAs were involved in the  
484 regulation of lung cancer development and progression.

485

486

487

488



489

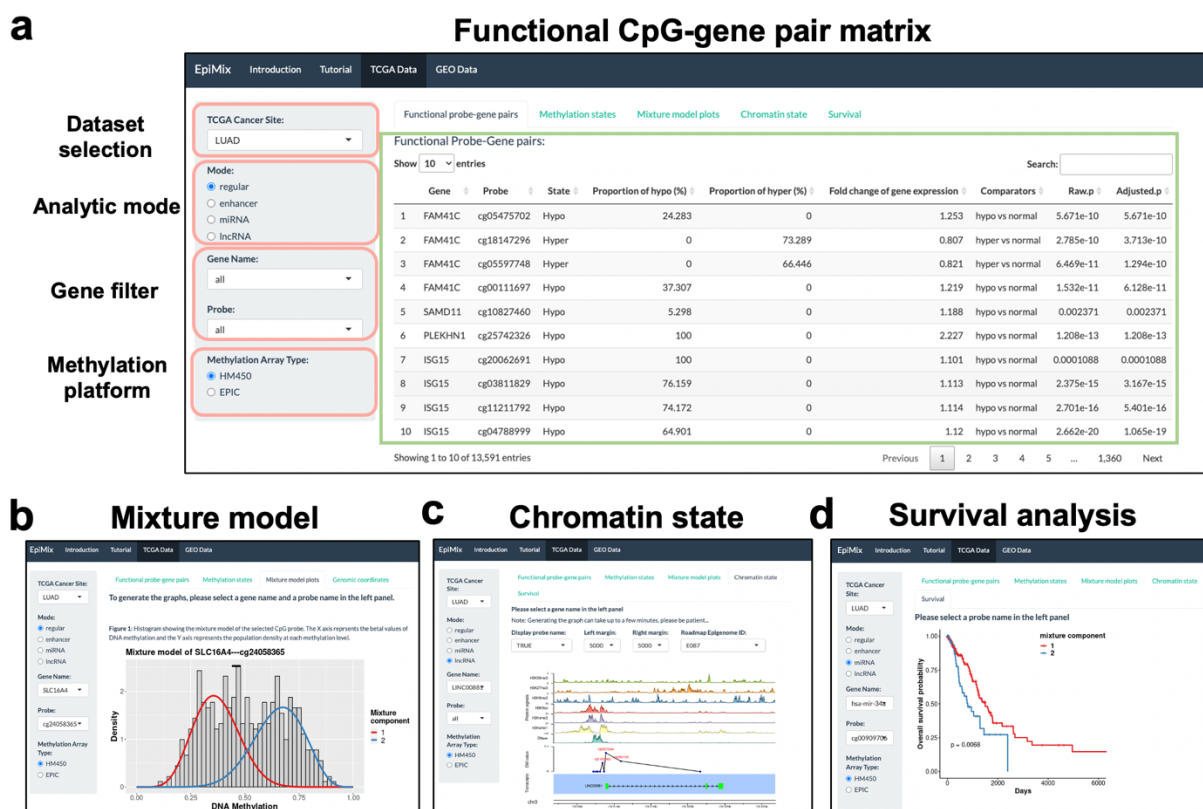
490 **Fig. 6 Identifications of differentially methylated lncRNA-coding genes in human lung cancers.** **a**,  
 491 Proportions of the hypo-, hyper- and dual methylated CpGs of lncRNA genes in epithelial cells from lung cancers  
 492 compared to normal tissues. **b-c**, Density plot showing the prevalence distribution of the **(b)** hypo- and **(c)**  
 493 hyper-methylated lncRNAs in the lung cancer cohort (n = 457). **d**, Mixture models of the *LINC00881* gene at two different  
 494 CpG sites. Red indicates normal methylation and blue indicates hypermethylation. **e**, Integrative visualization of  
 495 the transcript structure, DM values and chromatin state associated with the *LINC00881* gene. DM = 0: normal  
 496 methylation; DM > 0: hypermethylation. **f**, Kaplan-Meier survival curves of patients in the normally methylated and  
 497 the hypermethylated mixtures. Red indicates normal methylation and blue indicates hypermethylation. **g**,  
 498 Schematic representation of the DM value matrix. The rows correspond to CpG sites, and the columns correspond  
 499 component identified in the experimental group compared to the control group. At each CpG site, patients in  
 500 the same mixture component have the same DM values. DM < 0: hypomethylation, DM = 0: normal methylation, DM >  
 501 0: hypermethylation. **h**, Consensus matrix showing patient clusters based on the DM values of lncRNAs. **i**,  
 502 Proportions of male and female patients in different patient clusters (n1 = 120, n2 = 74, n3 = 72, n4 = 50, n5 = 133).  
 503 **j**, Kaplan-Meier survival curves of patients in different patient clusters. **k**, Top 20 enriched GO terms of the  
 504 methylation-driven lncRNAs in lung cancer. DM: differential methylation.

506

## 507 Discussion

508

509 In this study, we present EpiMix, a comprehensive analytic framework for population-  
 510 level analysis of DNAm and gene expression. We packaged the EpiMix algorithms  
 511 in R, enabling end-to-end DNAm analysis. To enhance the user experience, we also  
 512 implemented a web-based application (<https://epimix.stanford.edu>) for interactive  
 513 exploration and visualization of EpiMix's results (**Fig.7**). EpiMix contains diverse  
 514 functionalities, including automated data downloading, preprocessing, methylation  
 515 modeling and functional analysis. The seamless connection of EpiMix to data from the  
 516 TCGA program and the GEO database enables DNAm analysis on a broad range of  
 517 diseases. Here, we showed that EpiMix identified novel methylation-driven pathways  
 518 in food allergy and lung cancer. However, EpiMix is not limited to these disease areas  
 519 and can be easily applied to any other diseases.



520 Fig. 7 Screenshots of the EpiMix web application. **a**, Interactive data filters and visualization of functional CpG-  
 521 gene pair matrix. **b**, Visualization of the mixture model of the SLC16A4 gene in lung cancer. **c**, Genome-browser  
 522 style visualization of the lncRNA gene LINC00881 in lung cancer. **d**, Kaplan-Meier survival curves of patients with  
 523 different methylation states of the miRNA gene miR-34a in lung cancer.

524 EpiMix uses a beta mixture model to decompose the DNAm profiles in a patient  
525 population. Using EpiMix, we can resolve the epigenetic subtypes within the patient  
526 population and pinpoint the individuals carrying differential DNAm profiles. In this  
527 study, we identified five DNAm subtypes in lung cancers using the DM values of  
528 lncRNAs. Patients of subtype 2 had worse survival than patients of subtype 5,  
529 indicating that the DNAm subtypes discovered by EpiMix had prognostic values. The  
530 biological interpretation of DNAm subtypes requires the integration of data from other  
531 modalities, such as genetic mutations, lifestyle history, and other etiological features.

532

533 In addition, EpiMix was able to detect abnormal DNAm that was present in only small  
534 subsets of a patient cohort. In our simulation study, EpiMix detected more differentially  
535 methylated CpGs compared to existing methods, when the differential methylation  
536 occurred in only a small patient subset. Using the real lung cancer dataset ( $n = 457$ ),  
537 we identified miRNAs that were differentially methylated in only 1.1% of the patient  
538 population and lncRNAs differentially methylated in 0.6% of the patient population. We  
539 showed that over half of the miRNAs and lncRNAs were differentially methylated in  
540 only less than 20% of the patients. This unique feature of EpiMix to detect differential  
541 DNAm in small patient subsets enables us to identify novel epigenetic mechanisms  
542 underlying disease phenotypes. It can also be used to discover new epigenetic  
543 biomarkers and drug targets for improving personalized treatment.

544

545 Another feature of EpiMix is its ability to model DNAm at functionally diverse genomic  
546 elements. This includes *cis*-regulatory elements within or surrounding protein-coding  
547 genes, distal enhancers, and genes encoding miRNAs and lncRNAs. To model  
548 DNAm at distal enhancers, we selected the enhancers from the ENCODE and

549 ROADMAP consortiums, in which enhancers of over a hundred human tissues and  
550 cell lines were identified using the chromatin-state discovery (ChromHMM)<sup>59</sup>. Since  
551 enhancers are cell-type specific, EpiMix allows the users to select enhancers of  
552 specific cell types or tissues. In this study, we selected the enhancers of human blood  
553 and T cells, leading to the discovery of 40,311 CpG of enhancers. In addition to  
554 enhancers, many other regulatory elements were identified from the ROADMAP  
555 studies<sup>59</sup>. These include active transcription start site proximal promoters, zinc finger  
556 protein genes, bivalent regulatory elements, polycomb-repressed regions and many  
557 others. By customizing the “chromatin state” parameter of EpiMix, users can target the  
558 DNAm analysis to any of these regulatory modules.

559

560 Despite the critical biological functions of non-coding RNAs, there are no existing tools  
561 that specifically analyze DNAm regulating their transcription. To analyze DNAm of  
562 miRNA genes, we utilized the miRNA annotation from miRBase, the largest and  
563 consistently updated knowledge base of miRNAs<sup>60</sup>. In addition, we selected CpGs at  
564 miRNA promoters by using a recent database that integrates the information of miRNA  
565 TSSs from 14 genome-wide studies across different human cell types and tissues<sup>61</sup>.  
566 This led to the discovery of 17,192 CpGs associated with 1,484 miRNAs in the HM450  
567 array and 23,379 CpGs associated with 1,759 miRNAs in the EPIC array. With miRNA-  
568 Seq data provided, EpiMix can select differential DNAm that was associated with  
569 miRNA expression. Different from profiling protein-coding gene expression, measuring  
570 miRNA expression requires special library preparation strategies that capture small  
571 RNAs from total RNAs<sup>62</sup>. Users are preferentially needed to supply miRNA expression  
572 data obtained from proper library preparation strategies.

573

574 Similarly, custom methods are needed to accurately quantify lncRNA expression from  
575 RNA-Seq. We adopted the data processing pipeline developed from our previous  
576 study<sup>54</sup>. With this pipeline, we combined the transcriptome annotations from  
577 GENCODE and NONCODE. Raw sequencing reads were aligned to the combined  
578 transcriptome reference and quantified using the Kallisto-Sleuth algorithm<sup>56,57</sup>. Using  
579 this pipeline, we detected the expression of over 2,400 lncRNA genes. In this study,  
580 we have used our pipeline to generate lncRNA expression profiles for all the cancers  
581 in the TCGA database, and users can retrieve these data with EpiMix. Note, if users  
582 plan to use EpiMix on non-TCGA datasets, they are encouraged to use this pipeline  
583 to profile lncRNA expression.

584

585 Future work will aim to extend the use of EpiMix to whole-genome bisulfite sequencing  
586 and to further improve the scalability. Furthermore, the rapid development of single-  
587 cell technologies enables co-assay of DNAm and gene expression in thousands of  
588 cells. EpiMix can be used to identify differential DNAm that was present in only small  
589 subsets of a cell population. Therefore, a joint analysis of single cell methylome and  
590 transcriptome holds great promise for substantiating our goals, and the analytical  
591 framework presented here will be a valuable component for future research and  
592 applications.

593

## 594 **Methods**

595

### 596 **Data downloading**

597

598 The downloading module enables automated data downloading from the GEO  
599 database and TCGA project. Alternatively, users can supply custom datasets  
600 generated from their own studies. To retrieve data from GEO, we utilized the *getGEO*  
601 function from the GEOquery R package (version 2.62)<sup>63</sup>. In this study, we downloaded  
602 DNAm data and gene expression data using GEO accession number GSE114135.  
603 The DNAm data were beta values ranging from 0 to 1, representing the proportion of  
604 the methylated signal to the total signal. The gene expression data were TMM values.  
605 Other formats of gene expression data are also acceptable (e.g., RPKM, TPM, FPKM  
606 etc.). To retrieve data from TCGA, we used the Broad Institute Firehose tool  
607 (Firehose)<sup>64</sup>. We downloaded level three DNAm data and gene expression data. The  
608 downloaded data have been preprocessed for several steps, including removing  
609 problematic rows, removing redundant columns, reordering the columns and sorting  
610 the data by gene name. With the Regular mode, we used log-transformed RSEM  
611 values. With the miRNA mode, we used the pri-miRNA expression data with log-  
612 transformed RPKM values.

613

## 614 **Preprocessing**

615

616 The majority of datasets obtained from the TCGA and GEO databases have already  
617 been preprocessed for a few steps. EpiMix's contribution to preprocessing includes  
618 missing value imputation, removal of single-nucleotide polymorphism (SNP) probe  
619 and batch effect correction. Users can also select to remove CpGs on sex  
620 chromosomes. We then removed CpGs and samples with more than 20% missing  
621 values, and imputed missing values on the remaining dataset using the k-nearest  
622 neighbor (KNN) algorithm with  $K = 15$ .

623

624 Data from large patient cohorts were typically collected in technical batches.  
625 Systematic variances between technical batches may affect downstream data  
626 analysis and interpretation. To correct batch effects, we implemented two alternative  
627 approaches: (1) an anchor-based data integration approach adapted from the Seurat  
628 package (version 4.0.1)<sup>65</sup> and (2) an empirical Bayes regression approach, Combat<sup>66</sup>.  
629 The anchor-based approach uses canonical correlation analysis and mutual nearest  
630 neighbors to identify shared subpopulations (termed “anchors”) across different  
631 datasets and then uses a non-linear transformation to integrate the data. To identify  
632 the anchors, we used the “vst” method to select the top 10% variable features.  
633 Effective batch effect removal was confirmed using the PCA-based ANOVA analysis.  
634 Alternatively, the batch effect can be corrected with the Combat algorithm<sup>58</sup>. We found  
635 that the anchor-based approach was more time efficient compared to the Combat.  
636 When tested on the lung cancer dataset, the former approach completed the batch  
637 correction within 2 hours, whereas the Combat consumed more than 48 hours.

638

### 639 **CpG annotation and filtering**

640

#### 641 *Regular mode*

642

643 The Regular mode aims to model DNAm at cis-regulatory elements within or  
644 immediately surrounding protein-coding genes. We paired each CpG site to the  
645 nearest genes based on the hg38 manifest generated from Zhou et al.<sup>67</sup>. Unique CpG-  
646 gene pairs were identified, where a CpG was either within the gene body or at the  
647 immediately surrounding area. Users can restrict the analysis to the promoters,

648 defined as 2 kb upstream and 500 bp downstream (-2000bp ~ +500bp) of the  
649 transcription start sites (TSSs). TSS information was retrieved from Ensembl using the  
650 *biomaRt* R package (version 2.50.1)<sup>68</sup>.

651

### 652 *Enhancer mode*

653

654 The Enhancer mode aims to model DNAm specifically at distal enhancers. Therefore,  
655 we selected the distal CpGs that were at least 2 kb away from any known TSSs. Users  
656 can customize this distance based on their needs. To select the CpGs within  
657 enhancers, we used the enhancer database established from the ENCODE and  
658 ROADMAP consortiums, in which enhancers of over a hundred human tissues and  
659 cell lines were identified using the chromatin-state discovery (ChromHMM)<sup>59</sup>. We  
660 looked for the DNA elements associated with the chromatin states of active enhancers  
661 (“EnhA1” and “EnhA2”) and genic enhancers (“EnhG1” and “EnhG2”). Since  
662 enhancers are cell-type specific, EpiMix allows users to select enhancers of specific  
663 cell types or tissue groups. In this study, we selected the enhancers of human blood  
664 and T cells, leading to the discovery of 40,311 CpGs of enhancers. For each CpG, we  
665 retrieved 20 nearby genes as candidate genes targets. This gene number was  
666 determined by the previous studies showing that many of the enhancers can regulate  
667 a gene within a 10-gene distance<sup>29,69,70</sup>. Genes that are positively regulated by the  
668 enhancers should have a negative relationship between DNAm and gene  
669 expression<sup>36,71,72</sup>. Therefore, we performed a one-tailed Wilcoxon rank-sum test on  
670 each enhancer-gene pair to select the enhancers whose methylation states were  
671 inversely associated with the gene expression. The raw *P* value from the Wilcoxon  
672 rank-sum test was adjusted using a permutation approach<sup>73</sup>, where an empirical *P*

673 value was determined by ranking the raw  $P$  value in a set of permutation  $P$  values from  
674 testing the expression of a set of randomly selected 1,000 genes (**Supplementary**  
675 **Fig.2**).

676

677 *miRNA mode*

678

679 MicroRNAs are commonly classified into “intergenic” or “intronic” based on their  
680 genomic locations. Intergenic miRNAs are found at previously unannotated human  
681 genome and are transcribed from their own unique promoters as independent entities.  
682 In contrast, intronic miRNAs are believed to share promoters with their host genes and  
683 co-transcribed from respective hosts. Recent evidence shows that some intronic  
684 miRNAs can also be transcribed independently from their host genes, suggesting they  
685 have their own independent promoters<sup>74</sup>. To select CpGs associated with miRNAs,  
686 we used a combined strategy. First, we obtained the most recent annotation of  
687 miRNAs from miRBase (version 22.1)<sup>60</sup>. For each miRNA gene, we selected CpGs  
688 that were located within 5 kb upstream and 5 kb downstream. Second, we selected  
689 CpGs at miRNA promoters by using a recent database that integrates miRNA TSS  
690 information from 14 genome-wide studies across different human cell types and  
691 tissues<sup>61</sup>. We included CpGs located with miRNA promoters defined as 2000 bp  
692 upstream and 1000 bp downstream of the TSSs. This combined feature selection  
693 strategy resulted in the discovery of 17,192 CpGs associated with 1,484 miRNAs in  
694 the HM450 array and 23,379 CpGs associated with 1,759 miRNAs in the EPIC array.

695

696 *lncRNA mode*

697

698 The mechanisms for transcriptional regulation of lncRNAs are similar to protein-coding  
699 genes. We first selected lncRNA-coding genes using the GENCODE annotation  
700 (Version 36). We then selected CpGs associated with each lncRNA based on the  
701 hg38 manifest generated from Zhou et al.<sup>67</sup>. Unique CpG-gene pairs were identified,  
702 where a CpG was either located within the gene body or at the immediately  
703 surrounding area. This resulted in the discovery of 98,320 CpGs associated with  
704 11,280 lncRNAs in the HM450 array and 184,816 CpGs associated with 15,392  
705 lncRNAs in the EPIC array. Alternatively, users can select to focus the analysis at  
706 lncRNA promoters, defined as 2 kb upstream and 500 bp downstream (-2000bp ~  
707 +500bp) of the TSSs. The TSS information was retrieved from Ensembl using the  
708 *biomaRt* R package (version 2.50.1)<sup>68</sup>.

709

## 710 **CpG site clustering and smoothing (optional features)**

711

### 712 *Clustering*

713

714 Modeling the DNAm at all individual CpG sites can be computationally expensive. In  
715 addition, it can also lead to overfitting of DNAm data in identifications of patient  
716 subsets. Since the DNAm at adjacent CpGs are strongly correlated, we implemented  
717 an optional feature that allows users to group the correlated CpGs into CpG clusters.  
718 First, we used the average linkage hierarchical clustering algorithm to cluster CpGs of  
719 a single gene into clusters. Then we cut off the hierarchical tree at a Pearson  
720 correlation threshold of 0.4 to define CpG clusters and single CpG sites when they do  
721 not correlate with other sites. For each CpG site cluster, we used the mean levels of  
722 DNAm of the CpGs to represent the cluster DNAm, resulting in potentially multiple

723 CpG site clusters representing a single gene. The DNAm modeling can then be  
724 performed at each separate CpG site or CpG site cluster.

725

726 *Smoothing*

727

728 Smoothing is another technique frequently used in removing noise and increasing  
729 statistical power in analyzing whole-genome bisulfite sequencing data<sup>6</sup>. This  
730 technique estimates localized DNAm levels using data of adjacent CpGs at a user-  
731 specified genomic window. EpiMix allows users to smooth the DNAm data using local  
732 likelihood smoothing<sup>75</sup>. Since the number of CpGs is lower in array-based data than  
733 in bisulfite sequencing data, using smoothing on array-based data should be taken  
734 with cautions.

735

736 **Methylation modeling**

737

738 After preprocessing, the methylation data are beta values bounded between 0 and 1,  
739 representing the proportion of the methylated signal to the total signal. When the study  
740 population is large, the beta values can be assumed to come from multiple underlying  
741 probability distributions, in our case, beta distributions. To model the DNAm, we fit a  
742 beta mixture model to the methylation values at each CpG site (or CpG site cluster).  
743 Let  $y_i$  denote the beta value from subject  $i$  at a CpG site, where  $i \in \{1, \dots, n\}$ , and  $n$   
744 represents the total number of subjects. Let  $k$  denote the class membership of subject  
745  $i$ , where  $k \in \{1, \dots, K\}$ , and  $K$  represents the total number of components in the mixture.  
746 Assume subject  $i$  belongs to component  $k$  with probability  $\eta_k$ , we will have  $\sum_{k=1}^K \eta_k =$   
747 1. Subsequently, the likelihood contribution from subject  $i$  is:

748 
$$f(Y_i = y_i) = \sum_{k=1}^K \eta_k \frac{y_i^{\alpha_k-1} (1-y_i)^{\beta_k-1}}{B(\alpha_k, \beta_k)}$$

749

750 where  $B(\alpha_k, \beta_k) = \int_0^1 t^{\alpha_k-1} (1-t)^{\beta_k-1} dt$  is the beta function. Since the population  
751 contains  $n$  subjects, the log-likelihood for the complete dataset is

752 
$$l(\alpha, \beta, \eta) = \sum_{i=1}^n \log \{f(Y_i = y_i)\}$$

753 The goal of our modeling is to estimate the  $\alpha, \beta, \eta$  parameters of each component that  
754 best fit the methylation values. Let  $\theta = \{\alpha_1, \beta_1, \eta_1, \dots, \alpha_k, \beta_k, \eta_k\}$  be a vector of  
755 parameters that define the shape of each component in the mixture. We used the  
756 expectation–maximization (EM) algorithm<sup>76</sup> to iteratively maximize the log-likelihood  
757 and update the conditional probability that  $y_i$  comes from the  $k$  th component.

758

759 To determine the best number of components  $K$ , we used The Bayesian Information  
760 Criterion (BIC) for model selection and to avoid overfitting:

761 
$$BIC = \log(n) (3K) - 2 \times \sum_{i=1}^n \log \{f(Y_i = y_i)\}$$

762 This process involves iteratively adding a new mixture component if the BIC improves.  
763 Each mixture component represents a subset of samples for whom a particular  
764 DNAm state is observed.

765

## 766 **Identifications of differentially methylated CpGs**

767

768 If data of a control group are provided, we can determine whether a CpG site (or CpG  
769 site cluster) was hypo- or hyper-methylated by comparing its methylation levels in the

770 experimental group to its counterpart in the control group. We first performed beta  
771 mixture modeling on each CpG site (or CpG site cluster) to identify the mixture  
772 components using data from the experimental group, and the methylation levels of  
773 each of the mixture components were compared to the mean methylation levels of the  
774 control group. This methodology is based on the assumption that the DNAm profile  
775 is heterogenous across different subjects in the experimental (i.e., disease) group but  
776 is homogenous in the control group. For instance, the DNAm profile is expected to  
777 be different across cancer patients due to the difference in subtypes or driver  
778 mutations, but in normal tissues the DNAm should be relatively homogenous. In  
779 addition, the number of subjects in the experimental group is typically higher than the  
780 control group (e.g., TCGA projects). To determine the significant difference between  
781 the experimental and the control group, we used a Wilcoxon rank-sum to calculate the  
782 *P*-value, and multiple comparison was corrected with the false discovery rate (FDR).  
783 The *Q*-value threshold was set to 0.05. In addition, we required a minimum difference  
784 of 0.10 based on the platform sensitivity reported previously<sup>77</sup>.

785

### 786 **Identifications of differential DNAm that was associated with transcription**

787

788 If sample-matched gene expression data are provided, we can select the CpGs whose  
789 methylation states were significantly associated with gene expression. In this study,  
790 we focused on the identification of DNAm that represses gene expression. However,  
791 users have the option to identify DNAm that is positively correlated with gene  
792 expression. For each CpG-gene pair, we used a one-tailed Wilcoxon rank-sum test to  
793 compare the mean levels of gene expression in patients showing an abnormal  
794 methylation state (hypo- or hyper-methylation state) to those with a normal methylation

795 state. If a CpG was hypomethylated, we examined that the hypomethylated patients  
796 have higher gene expression levels compared to the normally methylated patients.  
797 Vice versa, if a CpG was hypermethylated, we tested that the hypermethylated  
798 patients have lower gene expression levels compared to the normally methylated  
799 patients. If a CpG was dual methylated (i.e., some samples were hypomethylated,  
800 while some others were hypermethylated), we tested that the hypomethylated patients  
801 have higher gene expression levels compared to the hypermethylated patients. Since  
802 a gene is typically paired with multiple CpGs, we adjusted the *P*-value using FDR to  
803 correct multiple comparisons. To select functionally significant CpG-gene pairs, we set  
804 the maximum threshold of the adjusted *P*-value to 0.01.

805

## 806 **Simulation study**

807

808 The goal of the simulation studies was to assess the sensitivity of EpiMix to detect  
809 differential DNAm present in only specific subsets of a population. The studies were  
810 performed by creating synthetic CpG sites and synthetic populations. First, we filtered  
811 CpGs showing statistically similar DNAm levels that fit a unimodal beta distribution  
812 from the activation group and from the quiescent group ( $n = 103$  samples per group).  
813 We then randomly sampled a subset of CpGs ( $n = 300$ ) from the quiescent group as  
814 the baselines. The average DNAm levels (beta values) of the CpGs in the baseline  
815 group ranged from 0.1 to 0.9, with a mean DNAm level of 0.6. Second, since the  
816 magnitude of changes in DNAm levels can be a critical factor affecting sensitivity, we  
817 created synthetic CpGs. For each CpG of the baseline group, we paired it with a  
818 subset of CpGs from the activation group, such that the differences in the mean beta  
819 values ( $\Delta\beta$ ) between the the activation group and the baseline group ranged from

820 0.1 to 0.7, where  $\Delta\beta \in \{0.10, 0.15, 0.20, 0.25, 0.30, 0.40, 0.50, 0.60, 0.70\}$ . This  
821 resulted in a total of 2,700 synthetic CpGs. Third, since our goal was to detect  
822 differential DNAm that was present in only a subset of the population, we created  
823 synthetic populations. For each synthetic CpG, we controlled the number of samples  
824 from the activation group to be combined with the baseline group, such that the final  
825 proportion ( $P$ ) of samples from the activation group in the combined datasets ranged  
826 from 0.01 to 0.50, where  $P \in$   
827  $\{0.01, 0.02, 0.05, 0.08, 0.10, 0.15, 0.20, 0.25, 0.30, 0.35, 0.40, 0.45, 0.50\}$ . Finally, we ran  
828 the EpiMix algorithm on each synthetic CpG and assessed whether it could pick up  
829 the differentially methylated signals in the synthetic populations.

830

### 831 **Benchmark with existing methods**

832

833 We benchmarked the performance of EpiMix with other existing methods, including  
834 Minfi<sup>10</sup>, iEVORA<sup>27</sup> and RnBeads<sup>12,28</sup>.

835

836 Minfi includes a differential methylation step based on an F-test. We first transformed  
837 beta values to M values, and the differential methylation analysis was performed with  
838 the *dmpFinder* function. We set the significant  $P$ -value and  $Q$ -value thresholds to 0.05.

839

840 iEVORA is a two-step algorithm that selects differentially variable and differentially  
841 methylated CpGs. The first step is to identify differentially variable CpGs using a  
842 Bartlett's test. The Bartlett's test assesses the equity of variances between the  
843 experimental and the control group. If in the experimental group, there are samples  
844 showing large differences (outliers) in DNAm versus other samples, the Bartlett's test

845 can detect such abnormality. The second step is to select the differentially variable  
846 CpGs that were also differentially methylated. The differential methylation analysis is  
847 performed by comparing the mean levels of DNAm of all the samples in the  
848 experimental group to the control group. We used the default parameters of the  
849 functions, with a Q-value (FDR) threshold of 0.001 for testing differential variability and  
850 *P*-value threshold of 0.05 for testing differential methylation means. In our stimulation  
851 studies, we found that iEVORA was able to identify differentially variable CpGs even  
852 when the abnormal methylation was present in only a small subset of the experimental  
853 group. However, since the algorithm does not identify which subjects were abnormally  
854 methylated, and in the differential methylation step, it still compares the mean levels  
855 of DNAm of the entire experimental group to the control group, the differential  
856 methylation test could not generate statistically significant results.

857

858 RnBeads uses hierarchical linear models as implemented in the limma package to  
859 identify differential methylated CpGs. We set the differential methylation *P*-value  
860 threshold to 0.05.

861

## 862 **Imputation of cell-type-specific DNAm and gene expression data**

863

864 DNAm and gene expression are known to be cell-type specific. When the DNAm  
865 were measured at the tissue (“bulk”) level, the differential DNAm profiles between  
866 patient subjects may result from the differences in tissue compositions. From a clinical  
867 perspective, tissue composition is meaningful in classifications of tumor subtypes and  
868 prediction of treatment response. However, from a biological perspective, users may  
869 be interested in identifying the differential DNAm present in specific cell types. EpiMix

870 focuses on the identification of differential DNAm across patient individuals. To  
871 resolve the confounding effect from tissue heterogeneity, we used previously validated  
872 algorithms to infer cell-type proportions and cell-type specific methylomes and  
873 transcriptomes (**Supplementary Fig.3**). First, we used CIBERSORTx<sup>45</sup>, a reference-  
874 based computational algorithm, to estimate cell-type proportions from bulk gene  
875 expression data in each tumor and normal tissue, and deconvolute bulk gene  
876 expression data into cell-type specific signals. This method leveraged the established  
877 signature gene expression matrices for experimentally purified cells from normal  
878 tissues and lung cancers<sup>45</sup>. Second, we used Tensor Composition Analysis (TCA)<sup>44</sup>  
879 to deconvolute bulk DNAm data into cell-type-specific data based on the estimated  
880 cell-type proportions in each tissue. The output from TCA was the methylome of each  
881 cell type in each individual. In addition to these methods, users can leverage other  
882 existing tools to adjust the effects from tissue compositions before inputting the data  
883 to EpiMix<sup>78-83</sup>.

884

### 885 **Genomic distribution of the differentially methylated CpGs**

886

887 Genomic coordinates of the TSSs of the methylation-driven genes were retrieved from  
888 Ensembl using the *biomaRt* R package (version 2.50)<sup>68</sup>. Exons and Introns of the  
889 protein-coding genes were retrieved from the TxDb object  
890 (*TxDb.Hsapiens.UCSC.hg38.knownGene*) (version 3.14)<sup>84</sup>. The GenomicRanges R  
891 package (version 1.46)<sup>85</sup> was used to identify the differentially methylated CpGs  
892 located within promoters, exons and introns.

893

### 894 **Motif enrichment analysis**

895

896 TF binding motifs were retrieved from HOCOMOCO, a comprehensive database for  
897 TF binding sites<sup>86</sup>. HOMER (Hypergeometric Optimization of Motif EnRichment) was  
898 used to find motif occurrences in a  $\pm 250$ bp region around each differentially  
899 methylated regions (DMRs). We then combined all the DMRs to identify enriched  
900 motifs. Enrichments were quantified using Fisher's exact test and multiple  
901 comparisons were adjusted with the Benjamini-Hochberg procedure. To calculate the  
902 enrichment Odds Ratio, we used all the distal CpGs as the background probes and  
903 the functional CpGs of enhancers as the target probes. We set the significant  $P$  value  
904 cutoff to 0.05 and the smallest lower boundary of 95% confidence interval for Odds  
905 Ratio to 1.1. The enrichment analysis was performed using the *get.enriched.motif*  
906 function from the *ELMER* library (version 3.14) in R<sup>11</sup>.

907

### 908 **Enrichment analysis of chromatin modifications**

909

910 Enrichment analysis of histone modifications at the DMRs was performed using the  
911 Genomic Hyperbrowser GSUITE of tools<sup>87</sup>. A suite of tracks representing different  
912 chromatin features for human naïve T cells (Epigenome ID: E038) and lung  
913 (Epigenome ID: E096) were retrieved from the ENCODE and ROADMAP  
914 consortiums<sup>59</sup>. To determine which tracks in the suite exhibit the strongest similarity  
915 by co-occurrence to the DMRs, the Forbes coefficient was used to obtain rankings of  
916 tracks, and Monte Carlo simulations were used to define a statistical assessment of  
917 the robustness of the rankings using randomization of genomic regions covered by  
918 the entire HM450 or EPIC array, and compute test statistics.

919

## 920 **Functional enrichment analysis**

921

922 Protein-coding genes

923

924 EpiMix provides an user interface to the *enrichGO* and *enrichKEGG* functions of the  
925 *clusterProfiler* R package (version 4.2.1)<sup>88</sup>. This enables gene set analysis of the  
926 methylation-driven genes using the gene ontology (GO) and KEGG datasets. Over-  
927 represented biological pathways in the methylation-driven genes were identified using  
928 the hypergeometric testing<sup>88</sup>. Enrichment results can be retrieved in a tabular format  
929 or visualized in several different ways. To perform the GO analysis, we set the  
930 significant *P* value to 0.05 and Q value to 0.20. Highly similar GO terms were removed  
931 with a cutoff *P* value of 0.60 to retain the most representative terms.

932

933 miRNAs

934

935 To obtain the target genes of the differentially methylated miRNAs, we queried  
936 miRTarBase with the *miRnetR* package<sup>89</sup>. Of the 144 differentially methylated miRNAs  
937 in lung cancer, we identified 7,088 target protein-coding genes of 26 miRNAs. We  
938 simplified this network by selecting the genes that were targeted by at least five  
939 miRNAs. KEGG pathway analysis was then performed on the miRNA target genes  
940 with hypergeometric testing.

941

942 lncRNAs

943

944 To carry out functional annotation and pathway analysis of the differentially methylated  
945 lncRNAs, we used the ncFANs V2.0 server (<http://ncfans.gene.ac/>)<sup>58</sup>. The genes in  
946 the significant CpG-gene pair matrix generated from EpiMix can be directly used as  
947 an input to ncFANs. NcFANs assigns the functions of protein-coding genes to lncRNAs  
948 based on pre-built co-expression networks in various normal tissues and cancers. We  
949 used the co-expression network built in the lung adenocarcinoma dataset from TCGA,  
950 and we set the correlation coefficient between lncRNAs and proteins-genes to 0.4 and  
951 the cutoff of the topological overlap measure similarity to 0.01.

952

### 953 **Biomarker identification and survival analysis**

954

955 Patient clinical data were retrieved from TCGA using the Firehose tool<sup>64</sup>. Alternatively,  
956 users can provide EpiMix with survival data if using their own datasets. We selected  
957 the CpGs with at least two methylation states. For each CpG, we fit a Cox proportional  
958 hazards regression model to assess the effect of methylation states on patient survival  
959 time. The log-rank test was used to compare the survival curve and to calculate the  
960 significant *P*-value.  $P < 0.05$  was considered as significant. The Kaplan-Meier survival  
961 plots were generated with the *survminer* R package (version 0.4.9).

962

### 963 **Genome browser-style visualization**

964

965 EpiMix enables genome browser-style visualization of the genomic coordinates and  
966 chromatin states of the differentially methylated genes and regions. We implemented  
967 two different forms of visualization. The gene-centric form shows the DM values of all  
968 the CpGs associated with a specific gene (e.g., **Fig.3f**). The CpG-centric form shows

969 a differentially methylated CpG and its upstream and downstream genes (e.g., **Fig.4e**).

970 Users can specify the number of nearby genes to display. Genes whose expression

971 levels were significantly associated with the DNAm levels of the CpG are shown in

972 red.

973

974 DNase I sensitivity and histone modification levels were retrieved from the ENCODE

975 and ROADMAP consortiums<sup>59</sup>. By providing the Epigenome ID, users can retrieve

976 data corresponding to the investigated tissue or cell type. In this study, we extracted

977 the chromatin features for human naïve T cells (Epigenome ID: E038) and fetal lung

978 (Epigenome ID: E088). The genomic coordinates (X-axis) were established on the

979 hg19 genome built, and the enrichment signal (Y-axis) represents negative log<sub>10</sub> of

980 the Poisson *P*-values. Human transcript annotation was retrieved from the TxDb object

981 (*TxDb.Hsapiens.UCSC.hg19.knownGene*) (version 3.2.2)<sup>90</sup>. The genomic coordinates

982 of the adjacent genes of the differentially methylated CpGs were retrieved from

983 Ensembl using the *biomaRt* R package (version 2.50.1)<sup>68</sup>. The visualization was

984 implemented with the *karyoploteR* package (version 1.20.0)<sup>91</sup>.

985

## 986 **Identifications of DNAm subtypes**

987

988 DNAm subtypes can be discovered by applying consensus clustering to the DM-

989 value matrix, where patients were clustered into robust and homogenous groups

990 (putative subtypes) based on their abnormal methylation profiles. Consensus

991 clustering was performed with the ConsensusClusterPlus R package (version

992 1.58.0)<sup>92</sup>. We used 1,000 rounds of k-means clustering and a maximum of  $K = 10$

993 clusters. Selection of the best number of clusters was based on the visual inspection  
994 of ConsensusClusterPlus output plots.

995

## 996 **Code availability**

997

998 EpiMix is available as an R package on Bioconductor  
999 (<https://bioconductor.org/packages/devel/bioc/html/EpiMix.html>). In addition, we also  
1000 developed a web application (<https://epimix.stanford.edu>) for users to interactively  
1001 visualize and explore the results from EpiMix.

1002

## 1003 **References**

- 1004 1. Li, J. *et al.* Insights Into the Role of DNA Methylation in Immune Cell  
1005 Development and Autoimmune Disease. *Front Cell Dev Biol* **9**, 757318 (2021).
- 1006 2. Si, J. *et al.* Epigenome-wide analysis of DNA methylation and coronary heart  
1007 disease: a nested case-control study. *eLife* vol. 10 Preprint at  
1008 <https://doi.org/10.7554/elife.68671> (2021).
- 1009 3. Zheng, Y., Luo, L., Lambertz, I. U., Conti, C. J. & Fuchs-Young, R. Early dietary  
1010 exposures epigenetically program mammary cancer susceptibility through Igf1-  
1011 mediated expansion of the mammary stem cell compartment. *Cells* **11**, 2558  
1012 (2022).
- 1013 4. Akalin, A. *et al.* methylKit: a comprehensive R package for the analysis of  
1014 genome-wide DNA methylation profiles. *Genome Biol.* **13**, R87 (2012).
- 1015 5. Park, Y. & Wu, H. Differential methylation analysis for BS-seq data under  
1016 general experimental design. *Bioinformatics* **32**, 1446–1453 (2016).

- 1017 6. Korthauer, K., Chakraborty, S., Benjamini, Y. & Irizarry, R. A. Detection and  
1018 accurate false discovery rate control of differentially methylated regions from  
1019 whole genome bisulfite sequencing. *Biostatistics* **20**, 367–383 (2019).
- 1020 7. Wang, X., Hao, D. & Kadarmideen, H. N. GeneDMRs: An R Package for Gene-  
1021 Based Differentially Methylated Regions Analysis. *J. Comput. Biol.* **28**, 304–316  
1022 (2021).
- 1023 8. Wang, D. *et al.* IMA: an R package for high-throughput analysis of Illumina’s  
1024 450K Infinium methylation data. *Bioinformatics* **28**, 729–730 (2012).
- 1025 9. Warden, C. D. *et al.* COHCAP: an integrative genomic pipeline for single-  
1026 nucleotide resolution DNA methylation analysis. *Nucleic Acids Res.* **41**, e117  
1027 (2013).
- 1028 10. Aryee, M. J. *et al.* Minfi: a flexible and comprehensive Bioconductor package for  
1029 the analysis of Infinium DNA methylation microarrays. *Bioinformatics* **30**, 1363–  
1030 1369 (2014).
- 1031 11. Silva, T. C. *et al.* ELMER v.2: an R/Bioconductor package to reconstruct gene  
1032 regulatory networks from DNA methylation and transcriptome profiles.  
1033 *Bioinformatics* **35**, 1974–1977 (2019).
- 1034 12. Müller, F. *et al.* RnBeads 2.0: comprehensive analysis of DNA methylation data.  
1035 *Genome Biology* vol. 20 Preprint at <https://doi.org/10.1186/s13059-019-1664-9>  
1036 (2019).
- 1037 13. Shaknovich, R. *et al.* DNA methylation signatures define molecular subtypes of  
1038 diffuse large B-cell lymphoma. *Blood* **116**, e81-9 (2010).
- 1039 14. Chen, X., Zhang, J. & Dai, X. DNA methylation profiles capturing breast cancer  
1040 heterogeneity. *BMC Genomics* **20**, 823 (2019).

- 1041 15. Schenkel, L. C. *et al.* DNA methylation epi-signature is associated with two  
1042 molecularly and phenotypically distinct clinical subtypes of Phelan-McDermid  
1043 syndrome. *Clin. Epigenetics* **13**, 2 (2021).
- 1044 16. Ghandi, M. *et al.* Next-generation characterization of the Cancer Cell Line  
1045 Encyclopedia. *Nature* **569**, 503–508 (2019).
- 1046 17. Partridge, E. C. *et al.* Occupancy maps of 208 chromatin-associated proteins in  
1047 one human cell type. *Nature* **583**, 720–728 (2020).
- 1048 18. Schoenfelder, S. & Fraser, P. Long-range enhancer–promoter contacts in gene  
1049 expression control. *Nat. Rev. Genet.* **20**, 437–455 (2019).
- 1050 19. Yao, L., Shen, H., Laird, P. W., Farnham, P. J. & Berman, B. P. Inferring  
1051 regulatory element landscapes and transcription factor networks from cancer  
1052 methylomes. *Genome Biol.* **16**, 105 (2015).
- 1053 20. Cribbs, A. P. *et al.* Methotrexate restores regulatory T cell function through  
1054 demethylation of the FoxP3 upstream enhancer in patients with rheumatoid  
1055 arthritis. *Arthritis rheumatol.* **67**, 1182–1192 (2015).
- 1056 21. Wang, L. *et al.* A MicroRNA Linking Human Positive Selection and Metabolic  
1057 Disorders. *Cell* **183**, 684-701.e14 (2020).
- 1058 22. Statello, L., Guo, C.-J., Chen, L.-L. & Huarte, M. Gene regulation by long non-  
1059 coding RNAs and its biological functions. *Nat. Rev. Mol. Cell Biol.* **22**, 96–118  
1060 (2021).
- 1061 23. Watanabe, K. *et al.* Genome structure-based screening identified epigenetically  
1062 silenced microRNA associated with invasiveness in non-small-cell lung cancer.  
1063 *Int. J. Cancer* **130**, 2580–2590 (2012).

- 1064 24. Zhang, M., Wu, J., Zhong, W., Zhao, Z. & He, W. DNA-methylation-induced  
1065 silencing of DIO3OS drives non-small cell lung cancer progression via activating  
1066 hnRNPK-MYC-CDC25A axis. *Mol Ther Oncolytics* **23**, 205–219 (2021).
- 1067 25. Gentleman, R. C. *et al.* Bioconductor: open software development for  
1068 computational biology and bioinformatics. *Genome Biol.* **5**, R80 (2004).
- 1069 26. Martino, D. *et al.* Epigenetic dysregulation of naive CD4+ T-cell activation genes  
1070 in childhood food allergy. *Nat. Commun.* **9**, 3308 (2018).
- 1071 27. Teschendorff, A. E. *et al.* DNA methylation outliers in normal breast tissue  
1072 identify field defects that are enriched in cancer. *Nat. Commun.* **7**, 10478 (2016).
- 1073 28. Assenov, Y. *et al.* Comprehensive analysis of DNA methylation data with  
1074 RnBeads. *Nat. Methods* **11**, 1138–1140 (2014).
- 1075 29. Mifsud, B. *et al.* Mapping long-range promoter contacts in human cells with high-  
1076 resolution capture Hi-C. *Nat. Genet.* **47**, 598–606 (2015).
- 1077 30. Javierre, B. M. *et al.* Lineage-Specific Genome Architecture Links Enhancers  
1078 and Non-coding Disease Variants to Target Gene Promoters. *Cell* **167**, 1369-  
1079 1384.e19 (2016).
- 1080 31. Jin, F. *et al.* A high-resolution map of the three-dimensional chromatin  
1081 interactome in human cells. *Nature* **503**, 290–294 (2013).
- 1082 32. Rao, S. S. P. *et al.* A 3D map of the human genome at kilobase resolution  
1083 reveals principles of chromatin looping. *Cell* **159**, 1665–1680 (2014).
- 1084 33. Sanyal, A., Lajoie, B. R., Jain, G. & Dekker, J. The long-range interaction  
1085 landscape of gene promoters. *Nature* **489**, 109–113 (2012).
- 1086 34. Bietz, A., Zhu, H., Xue, M. & Xu, C. Cholesterol Metabolism in T Cells. *Front.*  
1087 *Immunol.* **8**, 1664 (2017).

- 1088 35. Rasmussen, K. D. *et al.* TET2 binding to enhancers facilitates transcription  
1089 factor recruitment in hematopoietic cells. *Genome Res.* **29**, 564–575 (2019).
- 1090 36. Wang, L. *et al.* TET2 coactivates gene expression through demethylation of  
1091 enhancers. *Sci Adv* **4**, eaau6986 (2018).
- 1092 37. Li, P. *et al.* BATF–JUN is critical for IRF4-mediated transcription in T cells.  
1093 *Nature* **490**, 543–546 (2012).
- 1094 38. Glasmacher, E. *et al.* A Genomic Regulatory Element That Directs Assembly  
1095 and Function of Immune-Specific AP-1–IRF Complexes. *Science* vol. 338 975–  
1096 980 Preprint at <https://doi.org/10.1126/science.1228309> (2012).
- 1097 39. Furuta, M. *et al.* miR-124 and miR-203 are epigenetically silenced tumor-  
1098 suppressive microRNAs in hepatocellular carcinoma. *Carcinogenesis* **31**, 766–  
1099 776 (2010).
- 1100 40. Baer, C., Claus, R. & Plass, C. Genome-wide epigenetic regulation of miRNAs  
1101 in cancer. *Cancer Res.* **73**, 473–477 (2013).
- 1102 41. Cancer Genome Atlas Research Network. Comprehensive molecular profiling of  
1103 lung adenocarcinoma. *Nature* **511**, 543–550 (2014).
- 1104 42. Bloushtain-Qimron, N. *et al.* Cell type-specific DNA methylation patterns in the  
1105 human breast. *Proc. Natl. Acad. Sci. U. S. A.* **105**, 14076–14081 (2008).
- 1106 43. Schmidl, C. *et al.* Lineage-specific DNA methylation in T cells correlates with  
1107 histone methylation and enhancer activity. *Genome Res.* **19**, 1165–1174 (2009).
- 1108 44. Rahmani, E. *et al.* Cell-type-specific resolution epigenetics without the need for  
1109 cell sorting or single-cell biology. *Nat. Commun.* **10**, 3417 (2019).
- 1110 45. Newman, A. M. *et al.* Determining cell type abundance and expression from bulk  
1111 tissues with digital cytometry. *Nat. Biotechnol.* **37**, 773–782 (2019).

- 1112 46. Liang, G. *et al.* miR-196b-5p–mediated downregulation of TSPAN12 and  
1113 GATA6 promotes tumor progression in non-small cell lung cancer. *Proc. Natl.*  
1114 *Acad. Sci. U. S. A.* **117**, 4347–4357 (2020).
- 1115 47. Long, X. *et al.* MicroRNA-99a Suppresses Breast Cancer Progression by  
1116 Targeting FGFR3. *Front. Oncol.* **9**, 1473 (2019).
- 1117 48. Liu, L. *et al.* MicroRNA-29c functions as a tumor suppressor by targeting  
1118 VEGFA in lung adenocarcinoma. *Mol. Cancer* **16**, 50 (2017).
- 1119 49. Tang, R. *et al.* Downregulation of MiR-30a is Associated with Poor Prognosis in  
1120 Lung Cancer. *Med. Sci. Monit.* **21**, 2514–2520 (2015).
- 1121 50. Zhao, K. *et al.* Circulating microRNA-34 family low expression correlates with  
1122 poor prognosis in patients with non-small cell lung cancer. *J. Thorac. Dis.* **9**,  
1123 3735–3746 (2017).
- 1124 51. Chen, Y. *et al.* miRNA-148a serves as a prognostic factor and suppresses  
1125 migration and invasion through Wnt1 in non-small cell lung cancer. *PLoS One*  
1126 **12**, e0171751 (2017).
- 1127 52. Huang, H.-Y. *et al.* miRTarBase update 2022: an informative resource for  
1128 experimentally validated miRNA-target interactions. *Nucleic Acids Res.* **50**,  
1129 D222–D230 (2022).
- 1130 53. Derrien, T. *et al.* The GENCODE v7 catalog of human long noncoding RNAs:  
1131 analysis of their gene structure, evolution, and expression. *Genome Res.* **22**,  
1132 1775–1789 (2012).
- 1133 54. Zheng, H., Brennan, K., Hernaez, M. & Gevaert, O. Benchmark of long non-  
1134 coding RNA quantification for RNA sequencing of cancer samples. *Gigascience*  
1135 **8**, (2019).

- 1136 55. Fang, S. *et al.* NONCODEV5: a comprehensive annotation database for long  
1137 non-coding RNAs. *Nucleic Acids Res.* **46**, D308–D314 (2018).
- 1138 56. Bray, N. L., Pimentel, H., Melsted, P. & Pachter, L. Near-optimal probabilistic  
1139 RNA-seq quantification. *Nat. Biotechnol.* **34**, 525–527 (2016).
- 1140 57. Pimentel, H., Bray, N. L., Puente, S., Melsted, P. & Pachter, L. Differential  
1141 analysis of RNA-seq incorporating quantification uncertainty. *Nat. Methods* **14**,  
1142 687–690 (2017).
- 1143 58. Zhang, Y. *et al.* ncFANs v2.0: an integrative platform for functional annotation of  
1144 non-coding RNAs. *Nucleic Acids Res.* **49**, W459–W468 (2021).
- 1145 59. Roadmap Epigenomics Consortium *et al.* Integrative analysis of 111 reference  
1146 human epigenomes. *Nature* **518**, 317–330 (2015).
- 1147 60. Kozomara, A., Birgaoanu, M. & Griffiths-Jones, S. miRBase: from microRNA  
1148 sequences to function. *Nucleic Acids Res.* **47**, D155–D162 (2019).
- 1149 61. Wang, S., Talukder, A., Cha, M., Li, X. & Hu, H. Computational annotation of  
1150 miRNA transcription start sites. *Brief. Bioinform.* **22**, 380–392 (2021).
- 1151 62. Motameny, S., Wolters, S., Nürnberg, P. & Schumacher, B. Next generation  
1152 sequencing of miRNAs--strategies, resources and methods. *Genes* **1**, 70–84  
1153 (2010).
- 1154 63. Davis, S. & Meltzer, P. S. GEOquery: a bridge between the Gene Expression  
1155 Omnibus (GEO) and BioConductor. *Bioinformatics* **23**, 1846–1847 (2007).
- 1156 64. Center, B. I. T. G. D. A. Analysis-ready standardized TCGA data from Broad  
1157 GDAC Firehose 2016\_01\_28 run. *Broad Institute of MIT and Harvard* (2016).
- 1158 65. Stuart, T. *et al.* Comprehensive Integration of Single-Cell Data. *Cell* **177**, 1888-  
1159 1902.e21 (2019).

- 1160 66. Johnson, W. E., Li, C. & Rabinovic, A. Adjusting batch effects in microarray  
1161 expression data using empirical Bayes methods. *Biostatistics* **8**, 118–127  
1162 (2007).
- 1163 67. Zhou, W., Laird, P. W. & Shen, H. Comprehensive characterization, annotation  
1164 and innovative use of Infinium DNA methylation BeadChip probes. *Nucleic Acids*  
1165 *Res.* **45**, e22 (2017).
- 1166 68. Durinck, S., Spellman, P. T., Birney, E. & Huber, W. Mapping identifiers for the  
1167 integration of genomic datasets with the R/Bioconductor package biomaRt. *Nat.*  
1168 *Protoc.* **4**, 1184–1191 (2009).
- 1169 69. Ernst, J. *et al.* Mapping and analysis of chromatin state dynamics in nine human  
1170 cell types. *Nature* **473**, 43–49 (2011).
- 1171 70. Grubert, F. *et al.* Landscape of cohesin-mediated chromatin loops in the human  
1172 genome. *Nature* **583**, 737–743 (2020).
- 1173 71. Aran, D., Sabato, S. & Hellman, A. DNA methylation of distal regulatory sites  
1174 characterizes dysregulation of cancer genes. *Genome Biol.* **14**, R21 (2013).
- 1175 72. Cho, J.-W. *et al.* The importance of enhancer methylation for epigenetic  
1176 regulation of tumorigenesis in squamous lung cancer. *Exp. Mol. Med.* **54**, 12–22  
1177 (2022).
- 1178 73. Sham, P. C. & Purcell, S. M. Statistical power and significance testing in large-  
1179 scale genetic studies. *Nat. Rev. Genet.* **15**, 335–346 (2014).
- 1180 74. Ramalingam, P. *et al.* Biogenesis of intronic miRNAs located in clusters by  
1181 independent transcription and alternative splicing. *RNA* **20**, 76–87 (2014).
- 1182 75. Loader, C. *Local regression and likelihood*. (Springer, 1999).

- 1183 76. Dempster, A.P., Laird, N.M. and Rubin, D.B. Maximum likelihood from  
1184 incomplete data via the EM algorithm. *Journal of the Royal Statistical Society,*  
1185 *Series B (Methodological)*.
- 1186 77. Bibikova, M. *et al.* High-throughput DNA methylation profiling using universal  
1187 bead arrays. *Genome Res.* **16**, 383–393 (2006).
- 1188 78. Zou, J., Lippert, C., Heckerman, D., Aryee, M. & Listgarten, J. Epigenome-wide  
1189 association studies without the need for cell-type composition. *Nat. Methods* **11**,  
1190 309–311 (2014).
- 1191 79. Rahmani, E. *et al.* Sparse PCA corrects for cell type heterogeneity in  
1192 epigenome-wide association studies. *Nat. Methods* **13**, 443–445 (2016).
- 1193 80. Houseman, E. A. *et al.* Reference-free deconvolution of DNA methylation data  
1194 and mediation by cell composition effects. *BMC Bioinformatics* **17**, 259 (2016).
- 1195 81. Lutsik, P. *et al.* MeDeCom: discovery and quantification of latent components of  
1196 heterogeneous methylomes. *Genome Biol.* **18**, (2017).
- 1197 82. Teschendorff, A. E., Breeze, C. E., Zheng, S. C. & Beck, S. A comparison of  
1198 reference-based algorithms for correcting cell-type heterogeneity in Epigenome-  
1199 Wide Association Studies. *BMC Bioinformatics* **18**, 105 (2017).
- 1200 83. Rahmani, E. *et al.* BayesCCE: a Bayesian framework for estimating cell-type  
1201 composition from DNA methylation without the need for methylation reference.  
1202 *Genome Biol.* **19**, 141 (2018).
- 1203 84. Team, B. C. & Maintainer, B. P. TxDb. Hsapiens. UCSC. hg38. knownGene:  
1204 Annotation package for TxDb object (s). *R package* (2019).
- 1205 85. Lawrence, M. *et al.* Software for computing and annotating genomic ranges.  
1206 *PLoS Comput. Biol.* **9**, e1003118 (2013).

- 1207 86. Kulakovskiy, I. V. *et al.* HOCOMOCO: towards a complete collection of  
1208 transcription factor binding models for human and mouse via large-scale ChIP-  
1209 Seq analysis. *Nucleic Acids Res.* **46**, D252–D259 (2018).
- 1210 87. Simovski, B. *et al.* GSuite HyperBrowser: integrative analysis of dataset  
1211 collections across the genome and epigenome. *Gigascience* **6**, 1–12 (2017).
- 1212 88. Wu, T. *et al.* clusterProfiler 4.0: A universal enrichment tool for interpreting  
1213 omics data. *Innovation (N Y)* **2**, 100141 (2021).
- 1214 89. Chang, L., Zhou, G., Soufan, O. & Xia, J. miRNet 2.0: network-based visual  
1215 analytics for miRNA functional analysis and systems biology. *Nucleic Acids Res.*  
1216 **48**, W244–W251 (2020).
- 1217 90. Carlson, M. & Maintainer, B. Txdb. hsapiens. ucsc. hg19. knowngene:  
1218 Annotation package for txdb object (s). *R package version 3*, (2015).
- 1219 91. Gel, B. & Serra, E. karyoploteR: an R/Bioconductor package to plot  
1220 customizable genomes displaying arbitrary data. *Bioinformatics* **33**, 3088–3090  
1221 (2017).
- 1222 92. Wilkerson, M. D. & Hayes, D. N. ConsensusClusterPlus: a class discovery tool  
1223 with confidence assessments and item tracking. *Bioinformatics* **26**, 1572–1573  
1224 (2010).

1225

## 1226 **Acknowledgements**

1227 We thank Dr. Sandra Steyaert, Alexander Henry Thieme (Department of Radiation  
1228 Oncology, Charité - Universitätsmedizin Berlin), and Gautam Machiraju for helpful  
1229 comments and suggestions.

1230

## 1231 **Funding**

1232 Research reported here was further supported by the National Cancer Institute (NCI)  
1233 under awards: R01 CA260271, U01 CA217851 and U01 CA199241. The content is  
1234 solely the responsibility of the authors and does not necessarily represent the official  
1235 views of the National Institutes of Health.

1236

## 1237 **Author contributions**

1238 Y.Z: study design, implementation, data analysis and interpretation of results, draft  
1239 manuscript preparation

1240 J.J: implementation and data analysis

1241 K.B: study conception and design

1242 O.G: study conception and design, resources, supervision

1243

## 1244 **Competing interests**

1245 The authors declare no competing interests.